

1

2 The tumor suppressor APC is an attenuator of spindle-  
3 pulling forces during *C. elegans* asymmetric cell division

4

5

**-Author names and Affiliations**

6 Kenji Sugioka<sup>1,2,3</sup>, Lars-Eric Fielmich<sup>4</sup>, Kota Mizumoto<sup>2</sup>, Bruce Bowerman<sup>3</sup>, Sander  
7 van den Heuvel<sup>4</sup>, Akatsuki Kimura<sup>5,6</sup> and Hitoshi Sawa<sup>1,2,6</sup>

8

<sup>1</sup>Multicellular Organization Laboratory, National Institute of Genetics, 1111 Yata,  
9 Mishima, 411-8540 Japan

10

<sup>2</sup>RIKEN Center for Developmental Biology, 2-2-3 Minatojima-minamimachi, Chuo-  
11 ku, Kobe 650-0047 Japan

12

<sup>3</sup>Institute of Molecular Biology, University of Oregon, Eugene, OR 97403 USA

13

<sup>4</sup>Developmental Biology, Biology Department, Science 4 Life, Utrecht University,  
14 Padualaan 8,  
15 3584 CH, Utrecht, Netherlands

16

<sup>5</sup>Cell Architecture Laboratory, National Institute of Genetics, 1111 Yata,  
17 Mishima, 411-8540 Japan

18

<sup>6</sup>Department of Genetics, School of Life Science, Sokendai, 1111 Yata, Mishima,  
19 411-8540 Japan

20

21

**-Corresponding authors**

22

Hitoshi Sawa

1 Multicellular Organization Laboratory, National Institute of Genetics, 1111 Yata,  
2 Mishima, 411-8540 Japan  
3 hisawa@nig.ac.jp  
4 Phone: +81-55-981-6845  
5 Fax: +81-55-981-6846  
6  
7 Akatsuki Kimura  
8 Cell Architecture Laboratory, National Institute of Genetics, 1111 Yata,  
9 Mishima, 411-8540 Japan  
10 akkimura@nig.ac.jp  
11  
12 Sander van den Heuvel  
13 Developmental Biology, Biology Department, Utrecht University, Padualaan 8,  
14 3584 CH, Utrecht, Netherlands  
15 S.J.L.vandenHeuvel@uu.nl  
16  
17 Present address:  
18 Kota Mizumoto  
19 Department of Zoology, the University of British Columbia, Vancouver, Canada,  
20 V6T 1Z3  
21  
22

1 **Abstract**

2 The adenomatous polyposis coli (APC) tumor suppressor has dual functions in  
3 Wnt/ $\beta$ -catenin signaling and accurate chromosome segregation, and is frequently  
4 mutated in colorectal cancers. Although APC contributes to proper cell division, the  
5 underlying mechanisms remain poorly understood. Here we show that *C. elegans*  
6 APR-1/APC is an attenuator of the pulling forces acting on the mitotic spindle.  
7 During asymmetric cell division of the *C. elegans* zygote, a LIN-5/NuMA protein  
8 complex localizes dynein to the cell cortex to generate pulling forces on astral  
9 microtubules that position the mitotic spindle. We found that APR-1 localizes to the  
10 anterior cell cortex in a Par-aPKC polarity-dependent manner and suppresses anterior  
11 centrosome movements. Our combined cell biological and mathematical analyses  
12 support the conclusion that cortical APR-1 reduces force generation by stabilizing  
13 microtubule plus ends at the cell cortex. Furthermore, APR-1 functions in  
14 coordination with LIN-5 phosphorylation to attenuate spindle pulling forces. Our  
15 results document a physical basis for spindle-pulling force attenuation, which may be  
16 generally used in asymmetric cell division, and when disrupted potentially contributes  
17 to division defects in cancer.

18

19 **Significance Statement**

20 APC (adenomatous polyposis coli) is a Wnt signaling component as well as a  
21 microtubule-associated protein, and its mutations are frequently associated with  
22 colorectal cancers in humans. Although APC stabilizes microtubules (MTs), its  
23 mechanical role during cell division is largely unknown. Here we show that APC is an  
24 attenuator of forces acting on the mitotic spindle during asymmetric cell division of  
25 the *C. elegans* zygote. We performed live-imaging, laser-microsurgery, and numerical

1 simulation to show how APC suppresses spindle pulling force generation by  
2 stabilizing microtubule plus-ends and reducing microtubule catastrophe frequency on  
3 the cell cortex. Our study is the first example that shows the mechanical role of the  
4 APC protein, and provides a physical basis of spindle-pulling force attenuation.

5 \body

## 6 **Introduction**

7 The mitotic spindle segregates chromosomes and determines the plane of cell  
8 cleavage during animal cell division. Forces that act on the mitotic spindle regulate its  
9 position to produce daughter cells of the proper size, fate and arrangement, thereby  
10 playing a significant role in asymmetric cell division, tissue integrity and  
11 organogenesis. In various organisms, cells regulate spindle positioning through  
12 cortical force generators that pull on astral microtubules (Siller and Doe, 2009;  
13 Knoblich, 2010; Williams and Fuchs, 2013; Rose and Gönczy, 2014; di Pietro et al.,  
14 2016). An evolutionarily conserved force generator complex, consisting of LIN-  
15 5/NuMA, GPR-1,2/LGN and  $G\alpha$ , interacts with dynein and dynamic astral  
16 microtubules to position the mitotic spindle during the asymmetric divisions of the *C.*  
17 *elegans* early embryo (Rose and Gönczy, 2014), *Drosophila* and mammalian  
18 neuroblasts (Siller and Doe, 2009; Knoblich, 2010), and skin stem cells (Williams and  
19 Fuchs, 2013). Although Par-aPKC polarity and cell cycle regulators are known to  
20 control spindle positioning (Rose and Gönczy, 2014; Portegijs et al., 2016), how the  
21 forces are regulated spatiotemporally to position the spindle in various cell types  
22 during development remains poorly understood.

23 The tumor suppressor adenomatous polyposis coli (APC) is a widely  
24 conserved multifunctional protein with two major roles. First, APC functions as part  
25 of a degradation complex to down-regulate  $\beta$ -catenin-TCF dependent transcription,

1 thereby controlling cell fate and proliferation in various cell types (Clevers and Nusse,  
2 2012). Second, APC functions as a microtubule-associated protein to stabilize MTs. It  
3 has been suggested that this function of APC regulates cell migration (Barth et al.,  
4 2008; Etienne-Manneville, 2009), spindle orientation (Pereira and Yamashita, 2011;  
5 Yamashita et al., 2003), and chromosome segregation (Bahmanyar et al., 2009; Rusan  
6 and Peifer, 2008). In mammals, loss of the former function is closely associated with  
7 colon cancer (Moser et al., 1992; Su et al., 1992). Loss of the latter function causes  
8 spindle positioning defects (Beamish et al., 2009; Green et al., 2005) and  
9 chromosome instability (CIN) (Fodde et al., 2001; Green and Kaplan, 2003; Kaplan et  
10 al., 2001), a hallmark of metastatic tumors (Hanahan and Weinberg, 2011), suggesting  
11 that the cytoskeletal roles of APC during mitosis are also relevant for oncogenesis.  
12 How APC regulates the mitotic spindle remains poorly understood and is complicated  
13 by its multiple functions, binding-partners and cellular locations (Bahmanyar et al.,  
14 2009; Nelson and Näthke, 2013).

15 Yeast and fly studies have suggested that APC at the cell cortex contributes to  
16 mitotic spindle positioning. Kar9, a yeast protein with limited homology to APC,  
17 localizes asymmetrically to the cell cortex of budding daughter cells through type V  
18 myosin-dependent transport of growing microtubule ends (Hwang et al., 2003;  
19 Korinek et al., 2000; Lee et al., 2000). Cortical Kar9 captures microtubules (MTs) by  
20 binding yeast EB1, and promotes alignment of the spindle along the mother-bud axis  
21 (Miller and Rose, 1998; Korinek et al., 2000; Lee et al., 2000; Siller et al., 2006).  
22 *Drosophila* APC2 predominantly localizes to the cell cortex in syncytial embryos.  
23 APC2 mutants show a CIN phenotype, presumably because APC2 is required for  
24 proper centrosome separation (Poulton et al., 2013). The forces that mediate  
25 centrosome separation have been proposed to depend on APC2 connecting astral MTs

1 to cortical actin (Poulton et al., 2013). However, the mechanism by which cortical  
2 APC regulates spindle-pulling forces has not been directly addressed in any organism.

3 We report here that loss of cortical APR-1/APC disrupts asymmetries in  
4 spindle movements during mitotic division of the *C. elegans* zygote. In wild-type  
5 embryos, the net pulling forces acting on the mitotic spindle become higher in the  
6 posterior compared to the anterior, causing the spindle to move posteriorly during  
7 metaphase and anaphase (spindle displacement) (Galli and van den Heuvel, 2008;  
8 Gönczy, 2008). In anaphase, the posterior spindle pole swings along the transverse  
9 axis (spindle oscillation), while the anterior pole remains relatively stable. We found  
10 APR-1 to be enriched at the anterior cortex in a PAR-polarity dependent manner.  
11 Depletion of APR-1 resulted in anterior pole oscillations that resemble those of the  
12 posterior pole. Moreover, laser-mediated spindle severing showed that the spindle-  
13 pulling forces acting on the anterior spindle pole are increased in *apr-1(RNAi)*  
14 embryos. Using live imaging and numerical simulation, we found that the APR-1  
15 dependent stabilization of MT-cortex interactions negatively regulates the pulling  
16 forces acting on the anterior centrosome in wild-type zygotes. Our study identifies  
17 APR-1 as an attenuator of spindle-pulling forces, and improves our understanding of  
18 how cortical polarity precisely regulates spindle positioning during asymmetric cell  
19 division.

20

## 1 **Results and Discussion**

### 2 **APR-1/APC localizes asymmetrically to the cell cortex in a PAR and Frizzled** 3 **protein dependent manner**

4 We have previously shown that APR-1 localizes asymmetrically to the anterior cortex  
5 in the EMS blastomere at the six-cell stage and in post-embryonic seam cells, in  
6 response to Wnt signals that regulate the asymmetry of these divisions (Mizumoto and  
7 Sawa, 2007; Sugioka et al., 2011). While analyzing GFP::APR-1 localization in early  
8 embryos, we noticed that APR-1 is also asymmetrically localized in the zygote, called  
9 P0, where roles for Wnt signaling have not been reported. APR-1 formed dot-like  
10 particles that were enriched within the anterior cortex throughout P0 cell division  
11 (APR-1 asymmetry) (Figure 1A). We quantified the number of APR-1 dots by  
12 counting the fluorescent foci with a signal above a threshold (see Materials and  
13 methods). The foci numbers changed from prophase to metaphase, and from  
14 anaphase to telophase. Nevertheless, we observed anterior enrichment of APR-1 foci  
15 throughout mitosis (Figure 1A and 1D).

16 It is well-established that the Par-aPKC system generates anterior-posterior  
17 (A-P) cell polarity to regulate the asymmetric division of P0, through interactions  
18 between anterior (PAR-3, PAR-6, PKC-3) and posterior (PAR-2, PAR-1) *partitioning*  
19 *defective* (PAR) proteins at the cell cortex (Figure 1B; Munro and Bowerman, 2009).  
20 We found that APR-1 asymmetry in P0 was disrupted after RNAi knockdown of *par-*  
21 *3*, *pkc-3* or *par-2* (Figure 1C, 1E, and Figure S1), suggesting that its asymmetry is  
22 established through the Par-aPKC system.

23 In EMS and seam cells, the establishment of APR-1 asymmetry depends on  
24 Wnt proteins (Mizumoto and Sawa, 2007; Sugioka et al., 2011). In P0, MOM-2 is the  
25 only Wnt protein that is maternally provided as mRNA (Harterink et al., 2011),

1 although the mRNA appears not to be translated until the 4-cell stage (Oldenbroek et  
2 al., 2013). As expected, we found that APR-1 localization was not affected in *mom-*  
3 *2(or309)* null mutants, suggesting that the APR-1 asymmetry in P0 does not require  
4 Wnt ligands (Figure 1C, 1E, and Figure S1).

5         Despite the lack of a requirement for MOM-2/Wnt, we observed altered APR-  
6 1 localization after RNAi knockdown of downstream Wnt signaling components.  
7 Specifically, knockdown of the Frizzled receptor MOM-5 or simultaneous inhibition  
8 of the Dishevelled homologs, DSH-2 and MIG-5, increased the numbers of APR-1  
9 foci at metaphase/anaphase in both the anterior and posterior cortex without altering  
10 APR-1 expression levels (Figure 1C, 1E, Figure S1, and Figure S2A). Inhibition of  
11 WRM-1/ $\beta$ -catenin did not affect APR-1 localization, and *mom-5(RNAi)* as well as  
12 *dsh-2;mig-5(RNAi)* embryos still showed APR-1 asymmetry (Figure 1C, 1E, and  
13 Figure S1). DSH-2 localizes to the posterior cell cortex during Wnt-dependent  
14 asymmetric cell divisions later in development (Mizumoto and Sawa, 2007; Walston  
15 et al., 2004). In contrast, DSH-2 localization in P0 was not asymmetric (Figure S2B),  
16 consistent with the lack of Dishevelled requirement in APR-1 asymmetry.  
17 Interestingly, inhibition of the Axin homolog PRY-1 and Casein kinase homolog  
18 KIN-19 resulted in loss of APR-1 asymmetry only during meta-anaphase, suggesting  
19 their partial requirement in the establishment or maintenance of APR-1 asymmetry  
20 (Figure S1B and S1C). These results are consistent with observations at a later  
21 developmental stage (Baldwin and Phillips, 2014). We conclude that APR-1  
22 asymmetry in P0 is established by the Par-aPKC system with partial involvement of  
23 Axin and Casein kinase, while Frizzled and Dishevelled negatively regulate the levels  
24 of cortical APR-1.

25



## 1 **APR-1 asymmetrically suppresses centrosome movements during P0 cell division**

2 The Par-aPKC system independently regulates two P0 asymmetries: the segregation  
3 of cell fate determinants (e.g. PIE-1 and PGL-1) and posterior mitotic spindle  
4 displacement and thereby asymmetric cell cleavage. In *apr-1(RNAi)* embryos,  
5 GFP::PIE-1 segregated into the posterior daughter cell as in wild-type embryos,  
6 indicating that APR-1 is not involved in cytoplasmic determinant localization (Figure  
7 S2C). In contrast, *apr-1(RNAi)* embryos showed abnormal spindle oscillations. In  
8 wild type P0, posterior spindle displacement (represented by centrosome movements  
9 along the A-P axis) starts during metaphase and continues during anaphase when it  
10 coincides with transverse oscillations (represented by centrosome movements along  
11 the transverse axis) of the two spindle poles (Figure 2A, 2B, 2D, 2E). The posterior  
12 spindle pole oscillates more vigorously than the anterior pole (Figure 2B, 2E and  
13 Video 1), as a result of higher posterior than anterior cortical pulling forces (Pecreaux  
14 et al., 2006). In *apr-1(RNAi)* embryos, the mitotic spindle moved back and forth along  
15 the A-P axis (Figure 2C, 2D, and Video 2), and the anterior spindle pole exhibited  
16 excessive transverse oscillations, visible by the increased frequency and amplitude of  
17 the spindle pole tracks (Figure 2C, 2E and Video 2). As a result, the total distance  
18 traveled by the anterior centrosome significantly increased compared to that in control  
19 embryos (Figure 2F). These data indicate that APR-1 suppresses anterior spindle pole  
20 movements and thereby control spindle positioning during anaphase.

21 In *mom-5(ne12)* null mutant embryos, in which APR-1 levels were increased  
22 at both the anterior and posterior cortex, we observed reduced posterior spindle pole  
23 oscillations (Figure S3A and S3B). However, spindle pole oscillations were not  
24 restored in *apr-1(RNAi); mom-5(null)* embryos (Figure S3B). These results suggest  
25 APR-1-independent functions of MOM-5 that influence spindle movements. Because

1 of this, we could not determine the effects of excess cortical APR-1 on spindle pole  
2 movements in the *mom-5(null)* background. However, in other aspects of spindle  
3 dynamics described below, elevated cortical APR-1 localization potentiated APR-1  
4 function.

5

### 6 **APR-1 asymmetrically stabilizes microtubule-cortex interactions**

7 As mammalian APC (Zumbrunn et al., 2001) and *C. elegans* APR-1 in the EMS cell  
8 (Sugioka et al., 2011) can stabilize MTs, we hypothesized that anteriorly enriched  
9 APR-1 in the P0 cell may also increase MT stability at the cell cortex to regulate  
10 asymmetric spindle movements. To assess this possibility, we analyzed the MT-  
11 cortex interactions using live imaging of GFP:: $\beta$ -tubulin expressing embryos. In  
12 kymographs of midplane images, astral microtubules appear to persist longer on the  
13 anterior cell cortex than on the posterior, consistent with previous observations  
14 (Figure 3A; Labbé et al., 2003). To precisely quantify MT-plus end residence time at  
15 the cortex, we measured the duration of GFP:: $\beta$ -tubulin foci on the flattened cell  
16 surface (Figure 3B). Most of the GFP:: $\beta$ -tubulin foci initially co-localized with the  
17 EB1-related plus-end binding protein EBP-2 (96.1%; n = 255), confirming that the  
18 foci represent MT plus-ends. Shortly after the cortical attachment, EB1 dissociates  
19 from MT plus-ends, while some MTs remained at the cortex after the release of EB1  
20 (Fig. 3B and 3D). The numbers of such long-lived microtubule plus-ends were higher  
21 anteriorly, accounting for the asymmetry in cortical MT residence time in wild-type  
22 zygotes (Figure 3B-3D; red arrows in 3C, Video 3 and Video 4).

23 Notably, the MT residence time at the anterior cortex was significantly lower  
24 in *apr-1(RNAi)* embryos than in the wild type (Figure 3C, 3E and Video 5). In  
25 contrast, *mom-5* mutants with excess cortical APR-1 showed an increased MT

1 residence time at both the anterior and posterior cell cortex (Figure 3C, 3E and Video  
2 6). RNAi knockdown of *apr-1* overcame this *mom-5* phenotype, reducing MT cortical  
3 residence throughout the cortex (Figure 3C, 3E and Video 7). Thus, APR-1 stabilizes  
4 microtubule-cortex interactions and acts downstream of MOM-5 (Figure 4D).

5

### 6 **APR-1 asymmetrically attenuates pulling forces acting on the mitotic spindle**

7 The exaggerated anterior spindle pole movements in *apr-1(RNAi)* embryos implicate  
8 APR-1 in spindle-pulling force regulation. We investigated this possibility using  
9 spindle severing assays (Figure 4A; Grill et al., 2001). After cutting the spindle  
10 midzone with a UV laser, the average peak velocities of the anterior and posterior  
11 spindle poles moving toward the cell cortex were calculated (Figure 4A). In control  
12 embryos, the posterior spindle pole moved faster than the anterior pole, as expected  
13 (Figure 4A, 4B, and Video 8). In *apr-1(RNAi)* embryos, we observed an increased  
14 average peak velocity specifically for the anterior spindle pole (Figure 4A, 4B, and  
15 Video 8). In *mom-5(null)* embryos with excess cortical APR-1, both the anterior and  
16 posterior spindle poles showed reduced average peak velocities (Figure 4B and Video  
17 8). Combined *apr-1(RNAi);mom-5(null)* embryos showed increased average peak  
18 velocities and resembled *apr-1(RNAi)* embryos (Figure 4B and Video 8). These  
19 results indicate that the cortical levels of APR-1 inversely correlate with spindle-  
20 pulling forces and suggest a role for APR-1 as cortical pulling force attenuator (Figure  
21 4D).

22

23 **APR-1-dependent stabilization of MTs accounts for reduced pulling forces on**  
24 **the anterior spindle pole**

1 We have shown that APR-1 is enriched at the anterior cell cortex, promotes cortical  
2 MT residence times anteriorly, and suppresses both spindle-pulling forces and  
3 anterior spindle pole oscillations, raising the possibility that these processes are  
4 mechanistically linked. It has been shown that cortical pulling forces are generated  
5 when MTs reaching the cortex meet dynein and undergo catastrophe (Laan et al.,  
6 2012). Therefore, we hypothesized that cortical APR-1 reduces the MT catastrophe  
7 frequency and thereby attenuates force generation and spindle movement. However, it  
8 is not clear whether the magnitude of APR-1-dependent cortical MT stabilization is  
9 sufficient to suppress spindle movement.

10 We decided to examine this issue using numerical simulation. First, we  
11 estimated MT catastrophe frequencies from their cortical residence time  
12 (Supplementary Table 1, Figure S4). In control embryos, the estimated catastrophe  
13 frequency at the anterior cortex was about half of that at the posterior cortex. Such a  
14 reduced catastrophe frequency was not detected at the anterior cortex of *apr-1(RNAi)*  
15 embryos, indicating that in wild type embryos the catastrophe frequency is suppressed  
16 by APR-1.

17 We set the rescue frequency of all MTs high, so that soon after the MTs start  
18 to shorten, they regrow to reach the cortex (Supplemental Table 2). This assumption  
19 was introduced to make the number of MTs reaching the cortex almost constant  
20 regardless of the differences in catastrophe frequencies between anterior and posterior,  
21 which is the case in living embryos (Video 3). Without this assumption, the number  
22 of MTs reaching the cortex should be ~2-fold higher at the anterior because the  
23 catastrophe frequency is about half of the posterior catastrophe frequency. The  
24 mechanistic basis of this assumption is provided by the *in vivo* observation that  
25 individual microtubules appear to form bundles, and multiple EB1 tracks move along

1 a bundled fiber toward the cell cortex, making rescue frequency of the fiber higher  
2 than individual MTs (Video 4), which is consistent to the previous observation  
3 (Kozłowski et al., 2007).

4 We conducted 3-dimensional simulations of spindle movements. As in  
5 previous simulations (Hara and Kimura, 2009; Kimura and Onami, 2005, 2007;  
6 Kimura and Onami, 2010), the spindle moves as a result of three kinds of forces  
7 acting on astral MTs that radiate from each spindle pole (Figure 2G). First, all MTs  
8 generate pulling forces proportional to their length (“cytoplasmic pulling force”). This  
9 force is important for positioning of the spindle in the cell center during mitotic  
10 prophase (Hamaguchi and Hiramoto, 1986; Kimura and Onami, 2005; Kimura and  
11 Kimura, 2011), and is also critical for oscillation (Pecreaux et al., 2006). Second, MTs  
12 that reach the cell cortex generate the pulling force at their plus ends only when they  
13 undergo catastrophe (“cortical pulling force”). The current theory for the basis of  
14 oscillation is that when the spindle poles move toward one side, the pulling force from  
15 that side becomes stronger (“positive feedback” or “negative friction”), while the  
16 opposing centering force also increases (Grill et al., 2005; Pecreaux et al., 2006;  
17 Vogel et al., 2009). With this mechanism, the spindle is not stabilized at the center but  
18 oscillates. In our model, the frequency of the force generation depends on the number  
19 of active cortical force generators and the MT residence time controlled by APR-1,  
20 both of which have A-P asymmetry. The third force connects the anterior and  
21 posterior spindle poles. We assumed a spring-like connection between the poles that  
22 was weakened after anaphase onset to mimic the spindle elongation.

23 Numerical simulations were conducted for control, *apr-1(RNAi)*, and *mom-*  
24 *5(null)* situations (Figure S5), by setting the catastrophe frequency to values estimated  
25 from experimental data (e.g. 0.31 /s for the anterior and 0.72 /s for the posterior, see

1 Supplementary Table 1). The simulation results indicated that the APR-1-dependent  
2 stabilization of MTs is sufficient to suppress oscillation of the anterior pole (Figure  
3 2H). In wild-type simulations, the spindle moved toward the posterior and elongated  
4 upon anaphase onset (Figure S5A and Video 9). The oscillations perpendicular to the  
5 A-P axis were also reproduced for both spindle poles (Figure S5B). In *apr-1(RNAi)*  
6 simulations, in which the catastrophe frequency at the anterior cortex was increased,  
7 the amplitude of the anterior spindle pole oscillations was increased (Figure 2H,  
8 Figure S5 and Video 9). Furthermore, the average peak velocities of anterior poles in  
9 the severing experiments were also consistent with the forces acting on anterior  
10 spindle poles in our simulations (Figure 4C). Overall, the numerical simulations  
11 supported the hypothesis that the APR-1-dependent stabilization of MTs at the cortex  
12 can suppress spindle pole oscillations through the reduction of force generation.

13

#### 14 **Anterior APR-1 and LIN-5 phosphorylation together attenuate spindle pulling** 15 **forces**

16 We investigated the significance of spindle pulling force attenuators in asymmetric  
17 cell division. Along with APR-1, we focused on the LIN-5 protein. LIN-5 interacts  
18 with cortical GPR-1/2 and dynein in cortical force generation (Nguyen-Ngoc et al.,  
19 2007). We have previously reported that anteriorly-localized PKC-3/aPKC  
20 phosphorylates LIN-5 to attenuate cortical-pulling forces (Galli et al., 2011). We  
21 edited the *lin-5* genomic locus to substitute four aPKC phosphorylated serine residues  
22 with alanine by CRISPR/Cas9-mediated homologous recombination (*lin-5 4A*  
23 mutation). In spindle severing experiments, combining *apr-1(RNAi)* and the *lin-5 4A*  
24 mutation caused significantly enhanced average peak velocities of the anterior poles  
25 as compared to *apr-1(RNAi)* embryos (Figure 5A). Compared to *lin-5 4A* embryos,

1 the increase in anterior peak velocity was not significant ( $p= 0.07$ ; Figure 5A).  
2 However, in contrast to the single mutants, the ratio of anterior to posterior  
3 centrosome peak velocities in *apr-1(RNAi); lin-5 4A* double mutants was significantly  
4 reduced compared to wild-type controls (Figure 5B). These data suggest that the Par-  
5 aPKC-dependent asymmetric localization of APR-1 and phosphorylation of LIN-5  
6 together attenuate cortical pulling forces to generate pulling force asymmetry that  
7 positions the mitotic spindle (Figure 5C-5E).  
8

## 1 **Conclusion**

2 In this study, we investigated how the APR-1/APC protein regulates mitotic spindle  
3 movements in the *C. elegans* one-cell embryo, a well-established model for  
4 asymmetric cell division. We observed that APR-1/APC becomes asymmetrically  
5 enriched at the anterior cell cortex, dependent on the Par-PKC-3 polarity pathway.  
6 We found that APR-1 attenuates spindle pulling forces, most likely through  
7 stabilization of MTs at the anterior cell cortex. In concert, Wnt signaling components  
8 MOM-5/Frizzled and Disheveled proteins suppressed cortical accumulation of APR-1,  
9 thereby contributing to the correct levels of pulling forces. To test these assumptions,  
10 we performed numerical simulations, which closely mimicked the spindle movements  
11 in wild-type and mutant embryos. These combined data strongly support the  
12 conclusion that MT stabilization by APR-1 contributes to correct spindle positioning.  
13 Finally, we provide evidence to suggest that asymmetric APR-1 enrichment and PKC-  
14 3 phosphorylation of LIN-5 act in parallel to regulate asymmetric cell division. These  
15 conclusions are likely to apply broadly and improve our understanding of the  
16 microtubule-associated functions of APC.

17 Although APC is a component of Wnt signaling, its localization has been  
18 reported to be regulated by the Par-aPKC polarity pathway in migrating mammalian  
19 astrocytes (Etienne-Manneville and Hall 2003), and during axonal differentiation of  
20 developing hippocampal neurons (Shi et al., 2004), as we observed in the *C. elegans*  
21 one-cell embryo. Scratching of astrocyte monolayers in wound-healing assays triggers  
22 APC localization to the cell cortex at the leading edge, in response to CDC42-induced  
23 Par-aPKC polarity and Wnt5a signaling (Schlessinger et al., 2007). Interestingly,  
24 polarity establishment in this system is followed by centrosome re-orientation through  
25 APC-microtubule interactions (Etienne-Manneville and Hall 2003). Thus, the



1 mechanisms that control centrosome positioning through interactions between Par  
2 polarity, Wnt signaling, and APC may be conserved across species. The dynamic  
3 change in cortical APR-1 levels during P0 cell division is intriguing: this may reflect  
4 cell cycle dependent activation of the Wnt signaling pathway as reported in fly and  
5 mammalian cultured cells (Davidson et al., 2009).

6       While the roles of cortical APC have been unclear, it was previously proposed  
7 that APC stabilizes microtubules through microtubule plus-end binding protein EB1  
8 (Etienne-Manneville and Hall, 2003; Gundersen et al., 2004). Consistently, in the *C.*  
9 *elegans* EMS blastomere, cortical APC stabilizes MT ends coated with EB1 (Sugioka  
10 et al., 2011). However, a few examples including the present study indicate that  
11 cortical APC can stabilize microtubules independently of EB1. First, truncated  
12 mammalian APC that lacks the EB1 interaction domain has been shown to localize to  
13 the cell cortex and to MTs in epithelial cells (Reilein and Nelson, 2005). In addition,  
14 *Drosophila* APC2, which lacks the C-terminal EB1 binding domain, interacts with  
15 microtubule plus ends at the cortex and contributes to centrosome segregation  
16 (Poulton et al., 2013). In our study, APR-1 at the anterior cortex stabilizes MTs but  
17 the mean cortical residence time of EBP-2/EB1 was symmetric. We also observed  
18 that the cortical residence time of EB1 is much shorter than that of MTs in P0, as  
19 reported previously (Kozlowski et al., 2007). Therefore, APR-1 at the anterior cortex  
20 of P0 likely stabilizes MTs independently of EB1 binding. We observed recently that  
21 deleting all EB family members has limited effects on spindle behavior and viability  
22 in *C. elegans* (Schmidt et al., 2017). Therefore, the microtubule stabilizing effects of  
23 cortical APC probably do not depend on EB1 protein interactions.

24       Mitotic spindle positioning is tightly controlled during embryogenesis, in  
25 various adult stem cell divisions, and in symmetric divisions (Siller and Doe, 2009;

1 Williams and Fuchs, 2013; Kiyomitsu and Cheeseman, 2012). While many studies  
2 have focused on the localization of cortical force generators that pull on microtubule  
3 plus ends, attenuators of spindle pulling forces may be just as important in creating  
4 asymmetry. In fact, a variety of molecular mechanisms appear to suppress spindle  
5 pulling forces in the one-cell embryo, including PKC-3-mediated LIN-5  
6 phosphorylation (Galli et al., 2011), cortical actin (Berends et al., 2013), and  
7 posterior-lateral LET-99 localization (Krueger et al., 2010). This study provides  
8 insight into and a physical basis of spindle pulling force attenuation: we found that  
9 APC acts as an attenuator of spindle pulling forces, through stabilization of  
10 microtubule plus ends at the cortex. Importantly, a similar force attenuator function of  
11 APC is potentially used in oriented divisions of *Drosophila* germline stem cells  
12 (Yamashita et al., 2003), as well as mouse embryonic stem cells (ES cells) attached to  
13 Wnt-immobilized beads (Habib et al., 2013), as these systems exhibit asymmetric  
14 APC localizations similar to what we have observed in the *C. elegans* zygote. Our  
15 study also implies that not only APC but also other proteins involved in MT  
16 stabilization are potential cortical spindle pulling force attenuators.

17       The observed pulling force attenuation function may be relevant for the  
18 chromosomal instability (CIN) phenotype associated with APC loss in human colon  
19 cancer (Fodde et al., 2001; Kaplan et al., 2001). Initial studies of cultured mammalian  
20 cells associated APC loss and CIN with defective kinetochore-microtubule  
21 attachments, although abnormal spindle structures were also observed in APC  
22 defective cells (Fodde et al., 2001; Kaplan et al., 2001). In *Drosophila* embryos,  
23 APC2 was found to localize predominantly to the cell cortex (McCartney et al., 2001).  
24 Chromosome missegregation associated with APC2 loss in such embryos was linked  
25 to a cytoskeletal function of APC in centrosome segregation (Poulton et al., 2013). In

1 our study, we found that *C. elegans* APC localizes to the cell cortex where it  
2 negatively regulates spindle-pulling forces. Consequently, the absence of APC results  
3 in increased pulling forces exerted on the spindle poles. Interestingly, defective  
4 kinetochore attachments have been shown to cause chromosome segregation defects  
5 in *C. elegans*, in a manner dependent on cortical pulling forces (Cheeseman et al.,  
6 2005). Thus, combining these data with our results raises a new and testable  
7 hypothesis that increased cortical-pulling forces and abnormal MT-kinetochore  
8 interactions synergistically elevate the risk of CIN in developing tumors with APC  
9 mutations.

10

11

12

13

## 1 **Materials and methods**

### 2 ***C. elegans* culture and strains**

3 All strains used in this study were cultured by standard methods (Brenner, 1974).  
4 Most worms were grown at 20 °C or 22.5 °C and then incubated at 25 °C overnight  
5 before the analysis. Worms used for anti-DSH-2 staining were grown at 22.5 °C.  
6 Worms carrying PIE-1::GFP were grown at 15°C and incubated at 25°C overnight  
7 before the analysis. The following alleles were used: *mom-2(or309)*, *mom-5(ne12)*,  
8 *par-2(it51)*. We used *mom-5(ne12)* null mutants for all *mom-5* experiments except  
9 those in Figure 1. The following integrated transgenic lines were used: *osIs15*  
10 (Sugioka et al., 2011) for GFP::APR-1; *ruls32* (Praitis et al., 2001) for GFP::H2B;  
11 *ojIs1* (Strome et al., 2001) for GFP:: $\beta$ -tubulin; *axIs1462* (Merritt et al., 2008) for  
12 GFP::PIE-1; *axIs1720* (Merritt et al., 2008) for GFP::PGL-1; *tjIs8* for GFP::EBP-1;  
13 *ruls57* for GFP::tubulin. We also generated EBP-2::mKate2 fusion strain *ebp-*  
14 *2(or1954[ebp-2::mKate2])* and *lin-5 (he260[S729A,S734A,S737A,S739A])* strain by  
15 CRISPR/Cas9 genome editing as described below.

16

### 17 **Generation of CRISPR repair templates**

18 For the generation of the *ebp-2::mKate2* strain, CRISPR repair constructs containing  
19 700 bp homologous arms were synthesized as gBlock fragments (Integrated DNA  
20 Technologies, Coralville, IA) and assembled into pJET2.1 vector using in-house  
21 Gibson Assembly reaction mix (Gibson et al., 2009). For the generation of the *lin-5*  
22 *4A* strain, CRISPR repair constructs were inserted into the pBSK vector using Gibson  
23 Assembly (New England Biolabs, Ipswich, MA). Homologous arms of at least 1500  
24 bp upstream and downstream of the CRISPR/Cas9 cleavage site were amplified from  
25 cosmid C03G3 using KOD Polymerase (Novagen (Merck) Darmstadt, Germany).

1 Linkers containing the point mutations were synthesized (Integrated DNA  
2 technologies, Coraville, IA). Mismatches were introduced in the sgRNA target site to  
3 prevent cleavage of the repair template and knock-in alleles. All plasmids and primers  
4 used for this study are available upon request.

5

## 6 **CRISPR/ Cas9 genome editing**

7 Young adults were injected with solutions containing the following injection mix. For  
8 *ebp-2::mKate2*, 10 ng/μl pDD162 *Peft-3::Cas9* with sgRNA targeting C-terminus of  
9 *ebp-2* locus (Addgene 47549; Dickinson et al., 2013), 10 ng/μl repair template, and  
10 65 ng/μl selection marker pRF4 were used. For *lin-5* 4A, 50 ng/μl *Peft-3::Cas9*  
11 (Addgene 46168; Friedland et al., 2013), 50 ng/μl of two PU6::sgRNAs targeting the  
12 region of the four serine residues to be mutated to alanine, 50 ng/μl repair template  
13 and 2.5 ng/μl selection marker *Pmyo-2::tdTomato* were used. Progeny of animals that  
14 carry selection markers were transferred to new plates 3–4 days post injection. For  
15 *ebp-2::mKate2*, GFP positive animals were crossed with a strain carrying GFP::  
16 tubulin to obtain *ebp-2::mKate2* with GFP::tubulin (EU3068; *ebp-2(or1954[ebp-*  
17 *2::mKate2]* II). For *lin-5* 4A, PCRs with primers diagnostic for recombination  
18 products at the endogenous locus were performed on F2-F3 populations, where one  
19 primer targeted the altered base pairs in the sgRNA site and point mutations and the  
20 other just outside the homology arm. The resulting strain (SV1689; *lin-5*  
21 (*he260[S729A/S734A/S737A/S739A]* II) was crossed with AZ244 (*unc-119(ed3)*  
22 III; *ruIs57*) to obtain the *lin-5* 4A strain with GFP::tubulin (SV1690; *lin-5(he260);*  
23 *ruIs57*).

24

## 25 **RNAi**

1 DNA fragments corresponding to nucleotide 848-1547 of the *apr-1* cDNA were  
2 amplified and used for the production of the dsRNA and feeding RNAi. For the  
3 experiments in Figure 5, we injected the dsRNA into the gonad and worms were  
4 subsequently cultured under feeding RNAi at 25 °C for over 16 hrs before dissecting  
5 embryos. For the rest of experiments, after injection of the dsRNA into the gonad,  
6 worms were incubated at 25 °C without feeding RNAi for over 30 hrs before  
7 dissecting embryos.

8

### 9 **Microscopy and analysis of living embryos**

10 All embryos were dissected in an egg salt buffer from gravid hermaphrodites (Edgar,  
11 1995). For live imaging except for the experiments in Figure 5, the embryos were  
12 mounted on 4 % agar pads under a coverslip and sealed with petroleum jelly. For  
13 most of the experiments embryos were observed at room temperature by a CSU10  
14 spinning-disc confocal system (Yokogawa Electric, Musashino, Japan) mounted on an  
15 AxioPlan 2 microscope (Carl Zeiss, Oberkochen, Germany) with a Plan-Apochromat  
16 100X 1.4 NA oil immersion lens. The specimens were illuminated with a diode-  
17 pumped solid-state 488 nm laser (HPU50100, 20mW; Furukawa Electric, Tokyo,  
18 Japan). Images were acquired with an Orca ER12-bit cooled CCD camera  
19 (Hamamatsu Photonics, Hamamatsu, Japan), and the acquisition system was  
20 controlled by IP lab software (2 X 2 binning; Milwaukee, WI). Acquired images were  
21 processed with the Image J (Schneider et al., 2012) (NIH) and Adobe Photoshop  
22 (Adobe Systems, San Jose, CA). For the experiments in Figure 3B, images were  
23 captured with a confocal unit CSU-W with Borealis (Andor Technology, Belfast,  
24 Northern Ireland) and dual EMCCD cameras iXon Ultra 897 (Andor Technology)  
25 mounted on an inverted microscope Leica DMI8 (Leica Microsystems, Wetzlar,

1 Germany) controlled by Metamorph (Molecular Devices, Sunnyvale, CA). Spindle  
2 severing experiments were performed with a Micropoint system (Photonic  
3 instruments, St Charles, IL) equipped with a 2 mW pulsed nitrogen laser (model VL-  
4 337; Laser Science Inc., Franklin, MA) exciting Coumarin 440 dye. For the  
5 experiments in Figure 5, embryos were mounted on 4 % agarose pad dissolved in egg  
6 salts buffer and observed by a Nikon Eclipse Ti microscope with Perfect Focus  
7 System (Nikon, Tokyo, Japan) equipped with CSU-X1-A1 spinning disk confocal  
8 head (Yokogawa Electric) and S Fluor 100X 1.3 NA objectives. The specimens were  
9 illuminated with Cobolt Calypso 491 nm laser (Cobolt, Solna, Sweden). Spindle  
10 severing experiments were performed with 355 nm Q-switched pulsed lasers (Teem  
11 Photonics, Meylan, France) with ILas system (Roper Scientific France, Lisses,  
12 France/ PICT-IBiSA, Institut Curie). Temperature was maintained at 25°C by  
13 INUBG2E-ZILCS Stage Top Incubator (Tokai Hit, Fujinomiya, Japan) on the  
14 motorized stage MS-2000-XYZ with Piezo Top plate (ASI, Eugene, OR). Images  
15 were acquired with an Evolve 512 EMCCD camera (Photometrics, Tucson, AZ), and  
16 the acquisition system was controlled by MetaMorph (Molecular Devices).

17

## 18 **Immunostaining**

19 Embryos were fixed and stained with rabbit anti-DSH-2 antibody as described  
20 (Hawkins et al., 2005).

21

## 22 **Measurement of embryo volumes**

23 The volumes (V) of embryos were estimated from the measured embryo length (X)  
24 and width (Y). When three semi-axes of ellipsoid (embryo) in the x, y and z axes are  
25 defined as a, b and c, volume of ellipsoid  $V = 4/3\pi abc$ . With the assumption of equal

1 embryo width in the y and z axes, we estimated a, b and c as 0.5X, 0.5Y and 0.5Y and  
2 calculated V.

3

#### 4 **Statistical analysis**

5 For multiple comparisons, one-way ANOVA with Holm-Sidak's method and Kruskal-  
6 Wallis test followed by Dunn's multiple comparison test were performed for the data  
7 with normal distribution and skewed distribution (judged by F-test), respectively. No  
8 statistical method was used to predetermine sample size. The experiments were not  
9 randomized. The investigators were not blinded.

10

#### 11 **Quantification of the data from fluorescence images**

12 For the quantification of the number of dots formed by GFP::APR-1, 8 bit images  
13 were processed with Gaussian blur and segmented with the threshold that covers all  
14 the visible dots using Fiji. Then number of segments were counted by the Image J  
15 plug-in Analyze Particles. For the quantification of total APR-1 level in Figure S2A, 4  
16 successive focal planes including cell center and cell surfaces (corresponding to the  
17 upper half of the cell) were combined by the sum projection and average signal  
18 intensity of cell region was subtracted by that in the area devoid of embryos. For the  
19 generation of kymographs that show the centrosome movements along the anterior-  
20 posterior axis, (Figure 2B and 2C, left panels), we drew lines passing through both  
21 centrosomes (some centers are missing due to the transverse movements) and  
22 generated kymographs using Image J function Multi Kymograph. For the generation  
23 of kymographs that show centrosome movements along the transverse axis (Figure 2B  
24 and 2C, right panels), we first adjusted the center of the centrosome manually and  
25 drew a line that passes through the center of the anterior or posterior centrosome and



1 performed the same procedures. Note that kymographs are composed of linear pixels  
2 of each frame for all time points that together show the centrosome trajectory over  
3 time. For the quantification of spindle movements, the coordinates of the center of the  
4 centrosomes were analyzed with the Image J plug-in Manual Tracking. For the  
5 generation of kymographs of cortical microtubules, (Figure 3A), we extracted and  
6 straightened cortical regions and performed photo-bleach corrections (exponential fit  
7 method) by Image-J. The image color map was changed to mpi-inferno with Image-J.  
8 For the quantification of cortical residence times of GFP::EB1 and GFP:: $\beta$ -tubulin,  
9 the number of frames from appearance to disappearance of each dot were counted  
10 manually. Note that some MT dots whose start and end of cortical localization were  
11 unclear were not counted. The average peak velocity after spindle severing was  
12 calculated from the distance traveled by the centrosome center.

13

### 14 **3-dimensional simulation of spindle movement**

15 **Overview.** The simulations included 2 spindle poles connected by a spring with  
16 dynamic astral MTs inside a cell. The cell was simulated as an oval with a long axis  
17 of 50  $\mu\text{m}$  and two short axes of 30  $\mu\text{m}$ . The initial position of the spindle poles was  
18 set in the center of the cell and aligned along the long axis with the distance of 10 $\mu\text{m}$ ,  
19 which corresponds to the size of the spindle. The MTs grow and shrink from the  
20 spindle poles stochastically according to the dynamic instability. Depending on the  
21 length and configuration of the MTs, 3 kinds of forces act on spindle poles to move  
22 them as explained below. From an initial configuration, the configuration of the MTs  
23 and the spindle poles was calculated at successive time steps as conducted in previous  
24 simulations (Hara and Kimura, 2009; Kimura and Onami, 2005, 2007; Kimura and  
25 Onami, 2010). The parameters used are listed in Table S2.

1 **Force 1, cytoplasmic pulling forces.** All MTs generate pulling force proportional to  
2 their length. This force is important to bring the spindle at the cell center (Hamaguchi  
3 and Hiramoto, 1986; Kimura and Onami, 2005; Kimura and Kimura, 2011), and is  
4 also critical for oscillation (Pecreaux et al., 2006). The cytoplasmic pulling force  
5 generated for an  $i$ -th MT was modeled as  $F_{cytoplasm}(i) = D \times L(i) \times F_{FG}(i)$ , where  $D$  is  
6 the density of active force generators in the cytoplasm and  $L(i)$  is the length of the MT.  
7  $F_{FG}(i)$  is same as in the cortical pulling force. The direction of the force is the same as  
8 the direction of the MT. We note that the centering force required for oscillation can  
9 also be provided by a force that microtubules produce when they push against the  
10 cortex (Garzon-Coral et al., 2016) instead of the cytoplasmic pulling force. The  
11 detailed mechanisms (i.e. pulling or pushing) of the centering force do not affect the  
12 overall behavior of our model.

13 **Force 2, cortical pulling forces.** MTs that reached the cell cortex generate pulling  
14 forces toward their direction only when they start to shrink. The cortical pulling force  
15 generated for an  $i$ -th MT was modeled as  $F_{cortex}(i) = N_{potential}(i) \times P_{active}(i) \times F_{FG}(i)$ .  
16  $N_{potential}$  is the number of force generators that can potentially interact with the MT.  
17 We set this value at 30 for the posterior cortex and 15 for the anterior cortex. The  
18 experimental value of this parameter has not been investigated, but this number is  
19 consistent with a previous study estimating that the total number of force generators is  
20 less than 50 and the density is double at the posterior cortex compared to anterior  
21 cortex (Grill et al., 2003).  $P_{active}$  is the probability that the potentially interacting force  
22 generators are active. A critical assumption to generate robust oscillation here is to  
23 model this value high when the spindle pole is approaching the site of the force  
24 generator, and low when the spindle pole is leaving (Grill et al., 2005; Pecreaux et al.,  
25 2006). In the previous study (Pecreaux et al., 2006),  $P_{active}$  was defined as  $P_{active} =$

1  $p_{mean} + (f'/f_c) \times p_{mean} \times (1 - p_{mean}) \times v - \tau \times (f'/f_c) \times p_{mean} \times (1 - p_{mean}) \times a$ . For simplicity, we  
2 neglected the acceleration term ( $a$ ) and fixed the  $p_{mean}$  parameter to 0.5 to see the  
3 extensive oscillation (Pecreaux et al., 2006). We set  $f'/f_c = 4.0/V_{max}$ , and thus used  
4  $P_{active} = 0.5 + v/V_{max}$ . Here  $v$  is the velocity of the spindle pole toward the direction of  
5 the force generator on the cortex. When  $v < 0$ , we set  $P_{active} = 0$ .  $F_{FG}$  is formulated as  
6  $F_{FG} = F_{stall} (1 - v/V_{max})$  (Kimura and Onami, 2005; Pecreaux et al., 2006). When  $v > V_{max}$ ,  
7 we set  $F_{FG} = 0$ . In the simulation, force generation for shrinking MTs lasts for 100  
8 steps (1 s).

9 **Force 3, forces connecting the two poles.** To connect the anterior and posterior  
10 spindle poles, which is done by spindle MTs *in vivo*, we treated the spindle as a  
11 Hookean spring. The natural length increases proportionally from 10  $\mu\text{m}$  at time zero  
12 to 12  $\mu\text{m}$  at  $t = 100$  s, which is the onset of anaphase in the simulation. After the onset  
13 of anaphase, the natural length increases proportionally to 22  $\mu\text{m}$  at  $t = 200$  s. The  
14 spring constant is high (1 pN/ $\mu\text{m}$ ) so that the length of spindle is almost maintained to  
15 the natural length.

16

17

## 18 **Acknowledgements**

19 We thank Nancy Hawkins for the anti-DSH-2 antibody, the *Caenorhabditis* Genetics  
20 Center (funded by the NIH Office of Research Infrastructure Programs; P40  
21 OD010440) for strains. This work was supported by the Netherlands Organization for  
22 Scientific Research (NWO) research program 821.02.001 to SvdH, NIH grant  
23 R01GM049869 to B.B., by the Human Frontier Science Program and NIG-JOINT  
24 (2013-A60) to K.S., by the Uehara Memorial Foundation to H.S., and Grants-in-Aid

- 1 for Scientific Research from the Ministry of Education, Culture, Sports, Science, and
- 2 Technology of Japan to H.S (JP22127005) and A.K. (JP15H04732 and JP15KT0083).
- 3

## 1 **Figure legends**

### 2 **Figure 1. The Par-aPKC system and Frizzled signaling regulate APR-1**

#### 3 **asymmetric localization during zygote division**

4 (A) GFP::APR-1 signals on the cell surface in different mitotic stages. In the right  
5 panels, computationally detected APR-1 dots are shown (see Material and Methods).  
6 (B) APR-1 and PAR-6 localizations in the cell midplane during asymmetric cell  
7 division. Schematic drawing shows polarized protein localizations. (C) GFP::APR-1  
8 signals on the cell surface in *mom-2(null)* mutants and *mom-5*, *par-2* or *par-3* RNAi  
9 embryos. (D) Quantified numbers of GFP::APR-1 dots on the anterior and posterior  
10 cell cortex of wild-type embryos in different mitotic stages. n = 5, 10, 5 from left to  
11 right. (E) Quantified numbers of GFP::APR-1 dots at metaphase or anaphase in RNAi  
12 embryos. n = 10, 7, 10, 9, 10, 10, from left to right. Ends of whiskers indicate  
13 minimum or maximum values. Double asterisk, asterisk and n.s. indicates:  $p < 0.01$ ,  $p$   
14  $< 0.05$  and  $p > 0.05$  (One-way ANOVA with Holm-Sidak's multiple comparison test).  
15 Scale bars are 10  $\mu\text{m}$ .

16

### 17 **Figure 2. APR-1 asymmetrically suppresses centrosome movements during the**

#### 18 **P0 cell division**

19 (A) Schematic drawings of spindle movements along the A-P and transverse axes.  
20 Spindle displacement and oscillations contribute mainly to the movements along the  
21 A-P and transverse axes, respectively. Blue arrows and red arrowhead indicate  
22 centrosomes (gamma-tubulin) and chromosomes (Histone H2B), respectively. (B, C)  
23 Centrosome movements in A-P (left panels) and transverse (right panels) axes in  
24 control (B) and *apr-1(RNAi)*  $\pm$  40 second around anaphase onset (C). Kymographs  
25 (stack of line images of each time point) were made to show centrosome movements

1 along the A-P and transverse axes separately. (D, E) Anterior centrosome position  
2 during cell division along the A-P (D) and vertical axes (E). Cell centers are position  
3 zero. (F, H) Total distances for movements of the anterior and posterior poles in  
4 living embryos (F) and in 3D simulations (H). (G) Physical model used for 3D  
5 simulations. A and P indicate the anterior and posterior spindle poles harboring  
6 shrinking MTs (orange) and elongating MTs (blue). Red and black arrows indicate  
7 centrosome movements and cortical force generation. For each MT catastrophe at the  
8 cortex, the average pulling forces acting on a single MT at the posterior are stronger  
9 than those at the anterior, due to the different probabilities of MT-force generator  
10 interactions (see Materials and methods). Error bars show 95% CI. Double asterisk  
11 and n.s. indicates:  $p < 0.01$  and  $p > 0.05$  compared to control (Kruskal-Wallis test  
12 followed by Dunn's multiple comparison test). Scale bars indicate 5  $\mu\text{m}$ .

13

14 **Figure 3. APR-1 asymmetrically stabilizes microtubule-cortex interactions**

15 (A) Cortical MT dynamics. Cortical area outlined by the solid line in top figure was  
16 extracted, straightened, and corrected for photobleaching. This cortical area, depicted  
17 by the dotted line (middle), was used to generate a kymograph (bottom). Color code  
18 of the kymograph was changed to highlight MTs. (B) Measurement of cortical MT  
19 residence. The embryos were mounted on agarose pads and flattened by coverslips to  
20 visualize cortical microtubule ends in a single focal plane. Examples of short and  
21 long-lived foci were shown below with simultaneous imaging of GFP:: $\beta$ -tubulin and  
22 EB1::mKate2. (C) Cortical microtubule dots in the indicated genotypes during  
23 metaphase-anaphase. Images are max projection of cortical GFP:: $\beta$ -tubulin for 60  
24 frames (42 sec). Yellow and Magenta arrows indicate the MT dots whose residence  
25 time was shorter and longer than 2.1 sec, respectively. See also Video 3, 5-7. (D)

1 Distribution of quantified cortical MT or EB1 residence time in wild-type animals.  
2 (E) Mean cortical MT residence time of indicated genotypes.  $n = 47, 42, 77, 67, 64,$   
3  $61, 37, 44,$  from left to right. Error bars show 95% CI. Double asterisk and asterisk  
4 indicate:  $p < 0.01$  and  $p < 0.05$  compared to control (Kruskal-Wallis test followed by  
5 Dunn's multiple comparison test). Scale bars indicate  $2.5 \mu\text{m}$ .

6

7 **Figure 4 APR-1 asymmetrically attenuates pulling forces acting on the mitotic**  
8 **spindle**

9 (A) Spindle severing experiments. The midzones of mitotic spindles were severed by  
10 laser irradiation around anaphase onset (upper left panel). Upon spindle severing,  
11 spindle remnants moved at different velocities depending on the net strength of  
12 pulling forces (upper right panel). Montages of dissected spindle dynamics were  
13 shown in the bottom panels as DIC images; spindle poles devoid of yolk granules  
14 were indicated by arrowheads. (B) Average peak velocity of spindle poles after  
15 spindle severing. (C) The average of outward pulling forces over 5 sec from anaphase  
16 onset ( $t = 100$  s) for 20 independent simulations. Error bars show 95% CI. Double  
17 asterisk and asterisk indicate:  $p < 0.01$  and  $p < 0.05$  compared to control (one-way  
18 ANOVA with Holm-Sidak's method). (D) Summary of relationships between cortical  
19 APR-1 level, cortical MT residence, cortical MT catastrophe frequencies, and spindle  
20 pulling forces. Scale bars indicate  $10 \mu\text{m}$ .

21

22 **Figure 5 Anterior APR-1 enrichment and LIN-5 phosphorylation together**  
23 **attenuate spindle pulling forces to generate pulling force asymmetry**

24 (A, B) Average peak velocity of spindle poles (A) and their posterior/anterior ratio  
25 (B) after spindle severing. Error bars show 95% CI. Double asterisk and asterisk

1 indicate:  $p < 0.01$  and  $p < 0.05$  compared to control (one-way ANOVA with Holm-  
2 Sidak's method). (C) Three elementary processes used in the model described in the  
3 panel C. (1) aPKC-dependent LIN-5 phosphorylation results in the inhibition of force  
4 generation, (2) Cortical MT stabilization by APC reduces the MT catastrophe  
5 frequency and (3) MT shrinkage-dependent force generation is suppressed by step (2).  
6 (D) A schematic model of asymmetric spindle force regulation in P0 cell (see text).  
7 (E) A diagram of spindle pulling force regulation pathways at the anterior cell cortex.

8

9 **Figure S1. Temporal and genetic regulation of cortical GFP::APR-1 localization**

10 (A, C) Quantified numbers of GFP::APR-1 dots on the anterior and posterior cell  
11 cortex are shown for prophase, metaphase, anaphase and telophase of control and  
12 RNAi embryos. (B) APR-1 dots in the indicated RNAi experiments. Left and  
13 right panels are original and computationally segmented binary images, respectively.  
14 Ends of whiskers indicate minimum to maximum values. Double asterisk, asterisk and  
15 n.s. indicates:  $p < 0.01$ ,  $p < 0.05$  and  $p > 0.05$  (One-way ANOVA with Holm-Sidak's  
16 multiple comparison test). Scale bars indicate 10  $\mu\text{m}$ .

17

18 **Figure S2. Roles of Wnt signaling in P0 cell division**

19 (A) APR-1 level after RNAi experiments. GFP fluorescence signal intensity per area  
20 of the whole embryo including the cell cortex and cytoplasm were measured and  
21 shown. Signal in wild-type indicates autofluorescence. (B) Immunofluorescence  
22 images of the DSH-2 protein during P0 and EMS cell division. Blue is DAPI staining.  
23 In EMS, the DSH-2 protein is enriched at the cell boundary between EMS and P2  
24 (arrowheads) while no asymmetry was observed in P0. (C) Localization of the cell  
25 fate determinant GFP::PIE-1 in the indicated genotypes. Control and *apr-1(RNAi)*



1 shows PIE-1 enrichment in the posterior blastomere P1. In the *par-2* mutant, PIE-1  
2 asymmetry was lost. Scale bars indicate 10  $\mu$ m.

3

#### 4 **Figure S3. Effects of *mom-5(RNAi)* on spindle pole movements and embryo sizes**

5 (A) Kymographs of the spindle movements in *mom-5(RNAi)*. Kymographs were  
6 generated as in Figure 2. (B) Distance traveled by the anterior or posterior spindle  
7 pole. Total distance centrosome traveled for  $\pm 40$  sec and  $\pm 100$  sec from anaphase  
8 onset were shown for *in vivo* measurements (left) and 3D simulations (right). Error  
9 bars show 95% CI. Asterisk indicate  $p < 0.05$  compared to control (Kruskal-Wallis  
10 test followed by Dunn's multiple comparison test).

11

#### 12 **Figure S4. Estimation of microtubule catastrophe frequencies at the cortex**

13 (A) Frequencies of MT residence times at the cell cortex observed experimentally  
14 (histograms) and predicted from the estimated catastrophe frequencies (black lines).  
15 (B) Estimated catastrophe frequencies for indicated genotypes. The data is the same  
16 as in Supplementary Table 1.

17

18

#### 19 **Figure S5. Numerical simulation of spindle movements**

20 (A-D) Representative trajectories of the spindle poles in the simulation. The  
21 trajectories of the anterior (green) and posterior (red) poles are shown. Their midpoint  
22 (black) is also shown in (A and D). (A, B) Control condition. (C, D) *apr-1(RNAi)*  
23 condition. (A and D) Trajectories along A-P axis (x axis). (C and E) and those along  
24 an axis perpendicular to the x axis (y axis) are shown.

25

1

2 **Table 1. Estimated catastrophe frequencies of the microtubules at the cortex.**

3 When catastrophe occurs stochastically with the frequency of  $\lambda$ , the probability  
4 distribution of the cortical residency time will be  $P(t) = \lambda \exp(-\lambda t)$ . Therefore, the  
5 probability of observing cortical residency time between  $t_1$  and  $t_2$  will be  $P(t_1 \sim t_2) =$   
6  $\exp(-\lambda t_1) - \exp(-\lambda t_2)$ . We fitted the experimentally obtained probability distribution of  
7 the cortical MT residency time to this equation to estimate the catastrophe frequencies  
8 of the MTs at the cortex.

9

10 **Table 2. Parameter values used in the simulation.**

11

12 **Video 1. Spindle movements in a control embryo.**

13 An embryo expressing GFP-histone H2B and GFP- $\beta$ -tubulin is shown from  
14 metaphase to telophase

15

16 **Video 2. Spindle movements in an *apr-1(RNAi)* embryo.**

17 An embryo expressing GFP-histone H2B and GFP- $\beta$ -tubulin is shown from  
18 metaphase to telophase

19

20 **Video 3.  $\beta$ -tubulin localization at the cell cortex in a control embryo.**

21 An embryo expressing GFP-histone H2B and GFP- $\beta$ -tubulin is shown for 42 sec from  
22 metaphase to anaphase (judged by the chromosome) with 700 msec intervals. Yellow  
23 and Magenta arrows indicate the MT dots whose residence times were shorter and  
24 longer than 2.1 sec.

25

1 **Video 4. Simultaneous imaging of tubulin and EB1 localization in a control**  
2 **embryo.**

3 Anaphase GFP- $\beta$ -tubulin and EB1-mKate2 at the cell surface (upper panels) and in  
4 the midplane (bottom panels) were shown. Blue arrowheads in the bottom indicate  
5 two bundled MTs with multiple EB1 foci.

6

7 **Video 5.  $\beta$ -tubulin localization at the cell cortex in an *apr-1(RNAi)* embryo.**

8 An embryo expressing GFP-histone H2B and GFP- $\beta$ -tubulin is shown for 42 sec from  
9 metaphase to anaphase (judged by the chromosomes) with 700 msec intervals. Yellow  
10 and Magenta arrows indicate the MT dots whose residence times were shorter and  
11 longer than 2.1 sec.

12

13 **Video 6.  $\beta$ -tubulin localization at the cell cortex in a *mom-5(null)* embryo.**

14 An embryo expressing GFP-histone H2B and GFP- $\beta$ -tubulin is shown for 42 sec from  
15 metaphase to anaphase (judged by the chromosomes) with 700 msec intervals. Yellow  
16 and Magenta arrows indicate the MT dots whose residence times were shorter and  
17 longer than 2.1 sec.

18

19 **Video 7.  $\beta$ -tubulin localization at the cell cortex in an *apr-1(RNAi); mom-5(null)***  
20 **embryo.**

21 An embryo expressing GFP-histone H2B and GFP- $\beta$ -tubulin is shown for 42 sec from  
22 metaphase to anaphase (judged by the chromosomes) with 700 msec intervals. Yellow  
23 and Magenta arrows indicate the MT dots whose residence times were shorter and  
24 longer than 2.1 sec.

25

- 1 **Video 8. Spindle severing experiments.**
- 2 A DIC movies of indicated embryos during spindle severing experiments. Spindle
- 3 was irradiated by a laser when the chromosomes appeared to be separated (anaphase
- 4 onset).
- 5 **Video 9. An example of 3D simulation.**

## 1   **References**

2

- 3   1.    Bahmanyar, S., Nelson, W.J. & Barth, A.I. Role of APC and its binding  
4       partners in regulating microtubules in mitosis. *Advances in experimental*  
5       *medicine and biology* **656**, 65-74 (2009).
- 6   2.    Baldwin, A.T. & Phillips, B.T. The tumor suppressor APC differentially  
7       regulates multiple  $\beta$ -catenins through the function of axin and CKI $\alpha$  during *C.*  
8       *elegans* asymmetric stem cell divisions. *J Cell Sci* **127**, 2771–2781 (2014).
- 9   3.    Barth, A.I., Caro-Gonzalez, H.Y. & Nelson, W.J. Role of adenomatous  
10       polyposis coli (APC) and microtubules in directional cell migration and  
11       neuronal polarization. *Semin Cell Dev Biol* **19**, 245-251 (2008). doi:  
12       10.1016/j.semcdb.2008.02.003.
- 13 4.    Beamish, H., de Boer, L., Giles, N., Stevens, F., Oakes, V., and Gabrielli, B.  
14       Cyclin A/cdk2 regulates adenomatous polyposis coli-dependent mitotic  
15       spindle anchoring. *J Biol Chem* **284**, 29015-29023 (2009). doi:  
16       10.1074/jbc.M109.042820.
- 17 5.    Berends, C. W. H., Munoz, J., Portegijs, V., Schmidt, R., Grigoriev, I., Boxem,  
18       M., Akhmanova, A., Heck, A. J. R. & van den Heuvel, S. F-actin asymmetry  
19       and the endoplasmic reticulum-associated TCC-1 protein contribute to  
20       stereotypic spindle movements in the *Caenorhabditis elegans* embryo. *Mol.*  
21       *Biol. Cell* **24**, 2201–2215 (2013).
- 22 6.    Brenner, S. The genetics of *Caenorhabditis elegans*. *Genetics* **77**, 71-94  
23       (1974).

- 1 7. Cheeseman, I.M., MacLeod, I., Yates, J.R., Oegema, K. & Desai, A. The  
2 CENP-F-like proteins HCP-1 and HCP-2 target CLASP to kinetochores to  
3 mediate chromosome segregation. *Curr Biol* **15**, 771-777 (2005).
- 4 8. Clevers, H. & Nusse, R. Wnt/beta-catenin signaling and disease. *Cell* **149**,  
5 1192-1205 (2012). doi: 10.1016/j.cell.2012.05.012.
- 6 9. Davidson, G., Shen, J., Huang, Y. L., Su, Y., Karaulanov, E., Bartscherer, K.,  
7 Hassler, C., Stannek, P., Boutros, M. & Niehrs, C. Cell cycle control of wnt  
8 receptor activation. *Dev Cell* **17**, 788–99 (2009).
- 9 10. Dickinson, D.J., Ward, J.D., Reiner, D.J., & Goldstein, B. Engineering the  
10 *Caenorhabditis elegans* genome using Cas9-triggered homologous  
11 recombination. *Nat. Methods* **10**, 1028-1034. (2013)
- 12 11. di Pietro, F., Echard, A. & Morin, X. Regulation of mitotic spindle orientation:  
13 an integrated view. *EMBO Rep.* **17**, 1106–1130. (2016)
- 14 12. Edgar, L.G. Blastomere culture and analysis. *Methods Cell Biol* **48**, 303-321  
15 (1995).
- 16 13. Etienne-Manneville, S. APC in cell migration. *Advances in experimental*  
17 *medicine and biology* **656**, 30-40 (2009).
- 18 14. Etienne-Manneville, S. & Hall, A. Cdc42 regulates GSK-3 $\beta$  and adenomatous  
19 polyposis coli to control cell polarity. *Cell* **421**, 753-756 (2003).
- 20 15. Fodde, R., Kuipers, J., Rosenberg, C., Smits, R., Kielman, M., Gaspar, C., van  
21 Es, J.H., Breukel, C., Wiegant, J., Giles, R.H., Clevers, H.. Mutations in the  
22 APC tumour suppressor gene cause chromosomal instability. *Nat Cell Biol* **3**,  
23 433-438 (2001).

- 1 16. Friedland, A.E., Tzur, Y.B., Esvelt, K.M., Colaiacovo, M.P., Church, G.M.,  
2 and Calarco, J.A. Heritable genome editing in *C. elegans* via a CRISPR-  
3 Cas9 system. *Nat Methods* **10**, 741-743 (2013). doi: 10.1038/nmeth.2532.
- 4 17. Galli, M., Munoz, J., Portegijs, V., Boxem, M., Grill, S.W., Heck, A.J., and  
5 van den Heuvel, S. aPKC phosphorylates NuMA-related LIN-5 to position  
6 the mitotic spindle during asymmetric division. *Nat Cell Biol* **13**, 1132-1138  
7 (2011). doi: 10.1038/ncb2315.
- 8 18. Galli, M. & van den Heuvel, S. Determination of the cleavage plane in early *C.*  
9 *elegans* embryos. *Annu Rev Genet* **42**, 389-411 (2008). doi:  
10 10.1146/annurev.genet.40.110405.090523.
- 11 19. Garzon-Coral, H., Fantana, H. A. & Howard, J. A force-generating machinery  
12 maintains the spindle at the cell center during mitosis. *Science* **352**, 1124-  
13 1127. (2016).
- 14 20. Gibson, D.G., Young, L., Chuang, R.Y., Venter, J.C., Hutchison, C.A., 3rd, &  
15 Smith, H.O. Enzymatic assembly of DNA molecules up to several hundred  
16 kilobases. *Nat Methods* **6**, 343-345. (2009).
- 17 21. Gönczy, P. Mechanisms of asymmetric cell division: flies and worms pave the  
18 way. *Nat Rev Mol Cell Biol* **9**, 355-366 (2008). doi: 10.1038/nrm2388.
- 19 22. Green, R.A. & Kaplan, K.B. Chromosome instability in colorectal tumor cells  
20 is associated with defects in microtubule plus-end attachments caused by a  
21 dominant mutation in APC. *J Cell Biol* **163**, 949-961 (2003).
- 22 23. Green, R.A., Wollman, R. & Kaplan, K.B. APC and EB1 function together in  
23 mitosis to regulate spindle dynamics and chromosome alignment. *Mol Biol*  
24 *Cell* **16**, 4609-4622 (2005).

- 1 24. Grill, S., Kruse, K. & Jülicher, F. Theory of Mitotic Spindle Oscillations. *Phys*  
2 *Rev Lett* **94**, 1-4 (2005).
- 3 25. Grill, S.W., Gönczy, P., Stelzer, E.H. & Hyman, A.A. Polarity controls forces  
4 governing asymmetric spindle positioning in the *Caenorhabditis elegans*  
5 embryo. *Nature* **409**, 630-633 (2001).
- 6 26. Grill, S.W., Howard, J., Schäffer, E., Stelzer, E.H.K. & Hyman, A.A. The  
7 distribution of active force generators controls mitotic spindle position.  
8 *Science* **301**, 518-521 (2003).
- 9 27. Gundersen, G., Gomes, E. & Wen, Y. Cortical control of microtubule stability  
10 and polarization. *Curr Opin Cell Biol* **16**, 106-112 (2004). doi:  
11 10.1016/j.ceb.2003.11.010.
- 12 28. Habib, S.J., Chen, B.C., Tsai, F.C., Anastassiadis, K., Meyer, T., Betzig, E.,  
13 and Nusse, R. A localized Wnt signal orients asymmetric stem cell division in  
14 vitro. *Science* **339**, 1445-1448 (2013). doi: 10.1126/science.1231077.
- 15 29. Hamaguchi, M.S. & Hiramoto, Y. Analysis of the Role of Astral Rays in  
16 Pronuclear Migration in Sand Dollar Eggs by the Colcemid - UV Method.  
17 *Dev Growth Differ* **28**, 143-156 (1986).
- 18 30. Hanahan, D. & Weinberg, R.A. Hallmarks of cancer: the next generation. *Cell*  
19 **144**, 646-674 (2011). doi: 10.1016/j.cell.2011.02.013.
- 20 31. Hara, Y. & Kimura, A. Cell-size-dependent spindle elongation in the  
21 *Caenorhabditis elegans* early embryo. *Curr Biol* **19**, 1549-1554 (2009). doi:  
22 10.1016/j.cub.2009.07.050.
- 23 32. Harterink, M., Kim, D.H., Middelkoop, T.C., Doan, T.D., van Oudenaarden,  
24 A., and Korswagen, H.C. Neuroblast migration along the anteroposterior axis  
25 of *C. elegans* is controlled by opposing gradients of Wnts and a secreted



- 1 Frizzled-related protein. *Development* **138**, 2915-2924 (2011). doi:  
2 10.1242/dev.064733.
- 3 33. Hawkins, N.C., Ellis, G.C., Bowerman, B. & Garriga, G. MOM-5 frizzled  
4 regulates the distribution of DSH-2 to control *C. elegans* asymmetric  
5 neuroblast divisions. *Dev Biol* **284**, 246-259 (2005).
- 6 34. Hwang, E., Kusch, J., Barral, Y. & Huffaker, T.C. Spindle orientation in  
7 *Saccharomyces cerevisiae* depends on the transport of microtubule ends along  
8 polarized actin cables. *J Cell Biol* **161**, 483-488 (2003).
- 9 35. Kaplan, K.B., Burds, a.a., Swedlow, J.R., Bekir, S.S., Sorger, P.K., and  
10 Nätke, I.S. A role for the Adenomatous Polyposis Coli protein in  
11 chromosome segregation. *Nat Cell Biol* **3**, 429-432 (2001).
- 12 36. Kimura, A. & Onami, S. Computer simulations and image processing reveal  
13 length-dependent pulling force as the primary mechanism for *C. elegans* male  
14 pronuclear migration. *Dev Cell* **8**, 765-775 (2005).
- 15 37. Kimura, A. & Onami, S. Local cortical pulling-force repression switches  
16 centrosomal centration and posterior displacement in *C. elegans*. *J Cell Biol*  
17 **179**, 1347-1354 (2007).
- 18 38. Kimura, A. & Onami, S. Modeling microtubule-mediated forces and  
19 centrosome positioning in *Caenorhabditis elegans* embryos. *Methods Cell*  
20 *Biol* **97**, 437-453 (2010). doi: 10.1016/S0091-679X(10)97023-4.
- 21 39. Kimura, K. & Kimura, A. Intracellular organelles mediate cytoplasmic pulling  
22 force for centrosome centration in the *Caenorhabditis elegans* early embryo.  
23 *Proc Natl Acad Sci U S A* **108**, 137-142 (2011). doi:  
24 10.1073/pnas.1013275108.

- 1 40. Kiyomitsu, T. & Cheeseman, I.M. Chromosome- and spindle-pole-derived  
2 signals generate an intrinsic code for spindle position and orientation. *Nat Cell*  
3 *Biol* **14**, 311-317 (2012). doi: 10.1038/ncb2440.
- 4 41. Knoblich, J. Asymmetric cell division: recent developments and their  
5 implications for tumour biology. *Nat Rev Mol Cell Biol* **11**, 849-860 (2010).  
6 doi: 10.1038/nrm3010.
- 7 42. Korinek, W.S., Copeland, M.J., Chaudhuri, A. & Chant, J. Molecular linkage  
8 underlying microtubule orientation toward cortical sites in yeast. *Science* **287**,  
9 2257-2259 (2000).
- 10 43. Kozlowski, C., Srayko, M. & Nedelec, F. Cortical microtubule contacts  
11 position the spindle in *C. elegans* embryos. *Cell* **129**, 499-510 (2007).
- 12 44. Krueger, L., Wu, J., Tsou, M. & Rose, L. LET-99 inhibits lateral posterior  
13 pulling forces during asymmetric spindle elongation in *C. elegans* embryos. *J*  
14 *Cell Biol* **189**, 481-495 (2010). doi: 10.1083/jcb.201001115.
- 15 45. Laan, L., Pavin, N., Husson, J., Romet-Lemonne, G., van Duijn, M., Lopez,  
16 M.P., Vale, R.D., Julicher, F., Reck-Peterson, S.L., and Dogterom, M. Cortical  
17 dynein controls microtubule dynamics to generate pulling forces that position  
18 microtubule asters. *Cell* **148**, 502-514 (2012). doi: 10.1016/j.cell.2012.01.007.
- 19 46. Labbé, J.C., Maddox, P.S., Salmon, E.D. & Goldstein, B. PAR proteins  
20 regulate microtubule dynamics at the cell cortex in *C. elegans*. *Curr Biol* **13**,  
21 707-714 (2003).
- 22 47. Lee, L., Tirnauer, J.S., Li, J., Schuyler, S.C., Liu, J.Y., and Pellman, D.  
23 Positioning of the mitotic spindle by a cortical-microtubule capture  
24 mechanism. *Science* **287**, 2260-2262 (2000).

- 1 48. McCartney, B.M., McEwen, D.G., Grevengoed, E., Maddox, P., Bejsovec, a.,  
2 and Peifer, M. *Drosophila* APC2 and Armadillo participate in tethering  
3 mitotic spindles to cortical actin. *Nat Cell Biol* **3**, 933-938 (2001).
- 4 49. Merritt, C., Rasoloson, D., Ko, D. & Seydoux, G. 3' UTRs are the primary  
5 regulators of gene expression in the *C. elegans* germline. *Curr Biol* **18**, 1476-  
6 1482 (2008). doi: 10.1016/j.cub.2008.08.013.
- 7 50. Miller, R.K. & Rose, M.D. Kar9p is a novel cortical protein required for  
8 cytoplasmic microtubule orientation in yeast. *J Cell Biol* **140**, 377-390 (1998).
- 9 51. Mizumoto, K. & Sawa, H. Cortical beta-catenin and APC regulate asymmetric  
10 nuclear beta-catenin localization during asymmetric cell division in *C. elegans*.  
11 *Devl Cell* **12**, 287-299 (2007).
- 12 52. Moser, A.R., Dove, W.F., Roth, K.A. & Gordon, J.I. The Min (multiple  
13 intestinal neoplasia) mutation: its effect on gut epithelial cell differentiation  
14 and interaction with a modifier system. *J Cell Biol* **116**, 1517-1526 (1992).
- 15 53. Munro, E. & Bowerman, B. Cellular symmetry breaking during  
16 *Caenorhabditis elegans* development. *Cold Spring Harb Perspect Biol* **1**,  
17 a003400 (2009). doi: 10.1101/cshperspect.a003400.
- 18 54. Nelson, S. & Näthke, I.S. Interactions and functions of the adenomatous  
19 polyposis coli (APC) protein at a glance. *J Cell Sci* **126**, 873-877 (2013). doi:  
20 10.1242/jcs.100479.
- 21 55. Nguyen-Ngoc, T., Afshar, K. & Gönczy, P. Coupling of cortical dynein and G  
22 alpha proteins mediates spindle positioning in *Caenorhabditis elegans*. *Nat*  
23 *Cell Biol* **9**, 1294-1302 (2007).

- 1 56. Oldenbroek, M., Robertson, S.M., Guven-Ozkan, T., Spike, C., Greenstein, D.,  
2 and Lin, R. Regulation of maternal Wnt mRNA translation in *C. elegans*  
3 embryos. *Development* **140**, 4614-4623 (2013). doi: 10.1242/dev.096313.
- 4 57. Pecreaux, J., Röper, J.-C., Kruse, K., Jülicher, F., Hyman, A.a., Grill, S.W.,  
5 and Howard, J. Spindle oscillations during asymmetric cell division require a  
6 threshold number of active cortical force generators. *Curr Biol* **16**, 2111-2122  
7 (2006).
- 8 58. Pereira, G. & Yamashita, Y.M. Fly meets yeast: checking the correct  
9 orientation of cell division. *Trends Cell Biol* **21**, 526-533 (2011). doi:  
10 10.1016/j.tcb.2011.05.004.
- 11 59. Portegijs, V., Fielmich, L. E., Galli, M., Schmidt, R., Muñoz, J., van Mourik,  
12 T., Akhmanova, A., Heck, A. J. R., Boxem, M. & van den Heuvel, S..  
13 Multisite phosphorylation of NuMA-related LIN-5 controls mitotic spindle  
14 positioning in *C. elegans*. *PLoS Genet.* **12**, e1006291 (2016).  
15 doi:10.1371/journal.pgen.1006291
- 16 60. Poulton, J.S., Mu, F.W., Roberts, D.M. & Peifer, M. APC2 and Axin promote  
17 mitotic fidelity by facilitating centrosome separation and cytoskeletal  
18 regulation. *Development* **140**, 4226-4236 (2013). doi: 10.1242/dev.094425.
- 19 61. Praitis, V., Casey, E., Collar, D. & Austin, J. Creation of low-copy integrated  
20 transgenic lines in *Caenorhabditis elegans*. *Genetics* **157**, 1217-1226 (2001).
- 21 62. Reilein, A. & Nelson, W.J. APC is a component of an organizing template for  
22 cortical microtubule networks. *Nat Cell Biol* **7**, 463-473 (2005).
- 23 63. Rose, L. & Gönczy, P. Polarity establishment, asymmetric division and  
24 segregation of fate determinants in early *C. elegans* embryos. (December 30,

- 1           2014), *WormBook*, ed. The *C. elegans* Research Community, WormBook, doi:  
2           10.1895/wormbook.1.30.2
- 3   64.   Rusan, N.M. & Peifer, M. Original CIN: reviewing roles for APC in  
4           chromosome instability. *J Cell Biol* **181**, 719-726 (2008). doi:  
5           10.1083/jcb.200802107.
- 6   65.   Schlessinger, K., McManus, E. & Hall, A. Cdc42 and noncanonical Wnt  
7           signal transduction pathways cooperate to promote cell polarity. *J Cell Biol*  
8           **178**, 355-361 (2007). doi: 10.1083/jcb.200701083.
- 9   66.   Schmidt, R., Fielmich, L.E., Grigoriev, I., Katrukha, E.A., Akhmanova, A.A.,  
10           & van den Heuvel, S.J.L. Two populations of cytoplasmic dynein contribute to  
11           spindle positioning in *C. elegans* embryos. *J Cell Biol* **216**, 2777-2793 (2017).  
12           doi: 10.1083/jcb.201607038.
- 13   67.   Schneider, C.A., Rasband, W.S. & Eliceiri, K.W. NIH Image to ImageJ: 25  
14           years of image analysis. *Nat Methods* **9**, 671-675 (2012).
- 15   68.   Siller, K.H., Cabernard, C. & Doe, C.Q. The NuMA-related Mud protein  
16           binds Pins and regulates spindle orientation in *Drosophila* neuroblasts. *Nat*  
17           *Cell Biol* **8**, 594-600 (2006).
- 18   69.   Siller, K.H. & Doe, C.Q. Spindle orientation during asymmetric cell division.  
19           *Nat Cell Biol* **11**, 365-374 (2009). doi: 10.1038/ncb0409-365.
- 20   70.   Srinivasan, D.G., Fisk, R.M., Xu, H. & van den Heuvel, S. A complex of LIN-  
21           5 and GPR proteins regulates G protein signaling and spindle function in *C*  
22           *elegans*. *Genes Dev* **17**, 1225-1239 (2003).
- 23   71.   Strome, S., Powers, J., Dunn, M., Reese, K., Malone, C.J., White, J., Seydoux,  
24           G., and Saxton, W. Spindle dynamics and the role of gamma-tubulin in early  
25           *Caenorhabditis elegans* embryos. *Mol Biol Cell* **12**, 1751-1764 (2001).

- 1 72. Su, L.K., Kinzler, K.W., Vogelstein, B., Preisinger, A.C., Moser, A.R.,  
2 Luongo, C., Gould, K.A., and Dove, W.F. Multiple intestinal neoplasia caused  
3 by a mutation in the murine homolog of the APC gene. *Science* **256**, 668-670  
4 (1992).
- 5 73. Sugioka, K., Mizumoto, K. & Sawa, H. Wnt regulates spindle asymmetry to  
6 generate asymmetric nuclear  $\beta$ -catenin in *C. elegans*. *Cell* **146**, 942-954  
7 (2011). doi: 10.1016/j.cell.2011.07.043.
- 8 74. Vogel, S.K., Pavin, N., Maghelli, N., Julicher, F. & Tolic-Norrelykke, I.M.  
9 Self-organization of dynein motors generates meiotic nuclear oscillations.  
10 *PLoS Biol* **7**, e1000087 (2009). doi: 10.1371/journal.pbio.1000087.
- 11 75. Walston, T., Tuskey, C., Edgar, L., Hawkins, N., Ellis, G., Bowerman, B.,  
12 Wood, W., and Hardin, J. Multiple Wnt signaling pathways converge to orient  
13 the mitotic spindle in early *C. elegans* embryos. *Dev Cell* **7**, 831-841 (2004).
- 14 76. Williams, S.E. & Fuchs, E. Oriented divisions, fate decisions. *Curr Opin Cell*  
15 *Biol* **25**, 749-758 (2013). doi: 10.1016/j.ceb.2013.08.003.
- 16 77. Yamashita, Y.M., Jones, D.L. & Fuller, M.T. Orientation of asymmetric stem  
17 cell division by the APC tumor suppressor and centrosome. *Science* **301**,  
18 1547-1550 (2003).
- 19 78. Zumbunn, J., Kinoshita, K., Hyman, A.A. & Näthke, I.S. Binding of the  
20 adenomatous polyposis coli protein to microtubules increases microtubule  
21 stability and is regulated by GSK3 beta phosphorylation. *Curr Biol* **11**, 44-49  
22 (2001).
- 23  
24  
25

|    |   |
|----|---|
| 1  |   |
| 2  | <b>List of figures, tables and movies</b> |
| 3  | Figure 1-5                                |
| 4  | Table 1-2                                 |
| 5  | Video 1-9                                 |
| 6  | Figure S1                                 |
| 7  | Figure S2                                 |
| 8  | Figure S3                                 |
| 9  | Figure S4                                 |
| 10 | Figure S5                                 |

# Figure 1

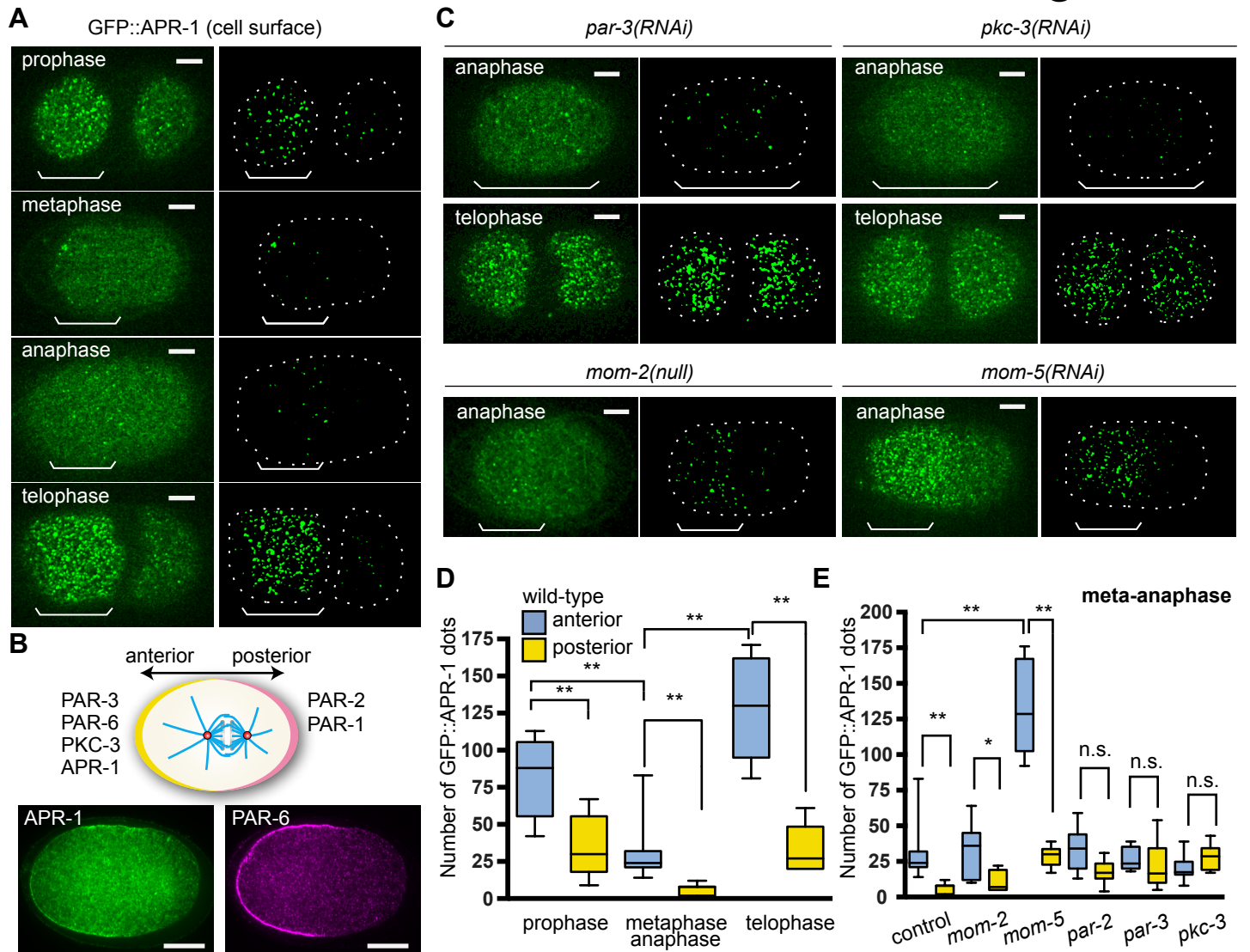


## Figure 1. The Par-aPKC system and Frizzled signaling regulate APR-1 asymmetric localization during zygote division.

(A) GFP::*APR-1* signals on the cell surface in different mitotic stages. In the right panels, computationally detected APR-1 dots are shown (see Material and Methods). (B) APR-1 and PAR-6 localizations in midplane during asymmetric cell division. Schematic drawing show polarized protein localizations. (C) GFP::*APR-1* signals on the cell surface in *mom-2*(null) mutants and *mom-5*, *par-2* or *par-3* RNAi embryos. (D) Quantified numbers of GFP::*APR-1* dots on anterior and posterior cell cortex of wild-type embryos in different mitotic stages.  $n = 5, 10, 5$  for each sample. (E) Quantified numbers of GFP::*APR-1* dots at metaphase or anaphase in RNAi embryos.  $n = 10, 7, 10, 9, 10, 10$ , from left to right. Ends of whiskers indicate minimum or maximum values. Double asterisk, asterisk and n.s. indicates:  $p < 0.01$ ,  $p < 0.05$  and  $p > 0.05$  (One-way ANOVA with Holm-Sidak's multiple comparison test). Scale bars are  $10\mu\text{m}$ .



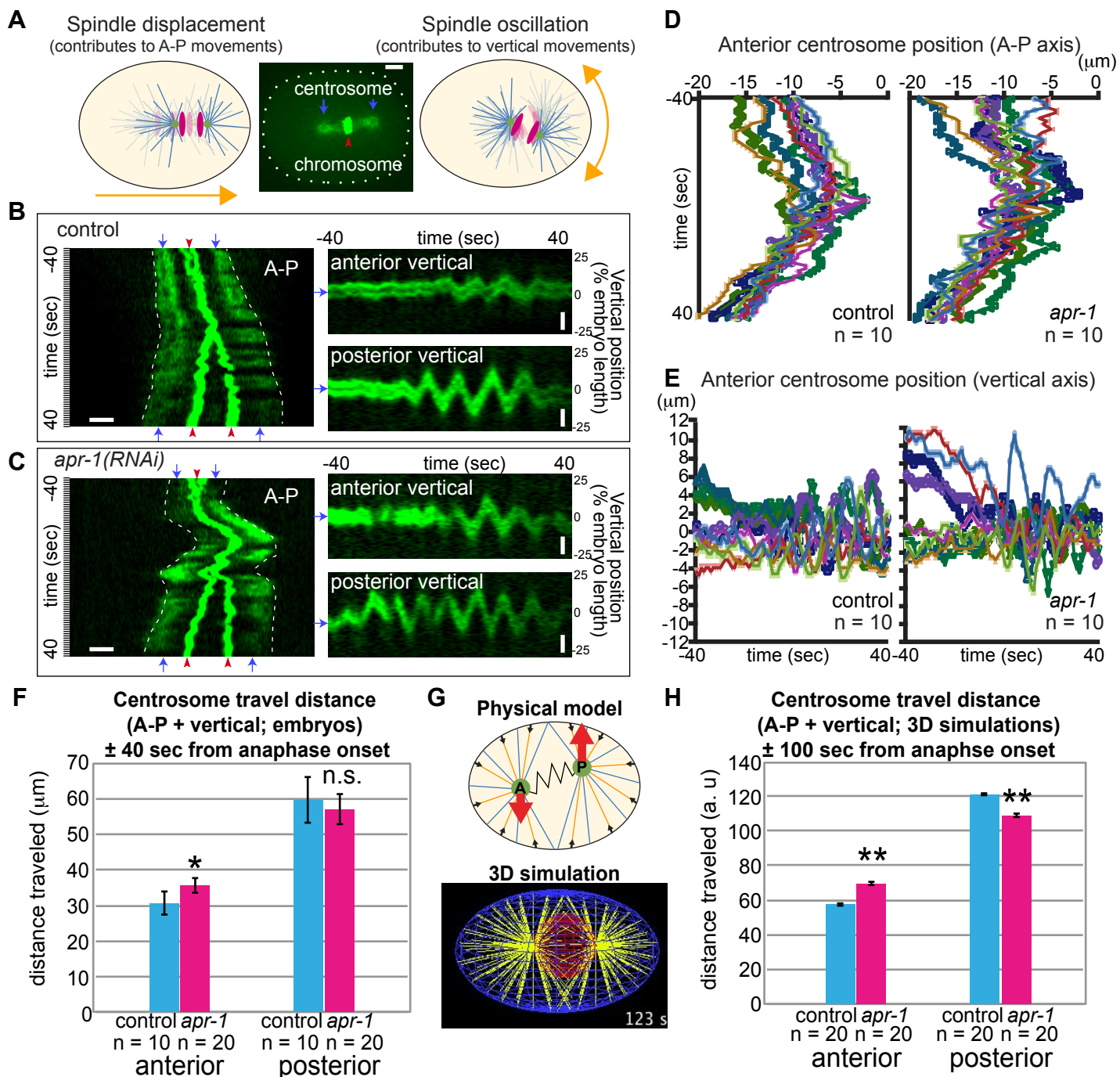


**Figure 2. APR-1 asymmetrically suppresses centrosome movements during the P0 cell division**

(A) Schematic drawings of spindle movements along the A-P and transverse axes. Spindle displacement and oscillations contribute mainly to the movements along the A-P and transverse axes, respectively. Blue arrows and red arrowhead indicate centrosomes (gamma-tubulin) and chromosomes (Histone H2B), respectively. (B, C) Centrosome movements in A-P (left panels) and transverse (right panels) axes in control (B) and *apr-1(RNAi)* (C). Kimographs (stack of line images of each time point) were made to show centrosome movements along the A-P and transverse axes separately. (D, E) Anterior centrosome position during cell division along the A-P (D) and vertical axes (E). Cell centers are position zero. (F, H) Total distances for movements of the anterior and posterior poles in living embryos (F) and in 3D simulations (H). (G) Physical model used for 3D simulations. A and P indicate the anterior and posterior spindle poles harboring shrinking MTs (orange) and elongating MTs (blue). Red and black arrows indicate centrosome movements and cortical force generation. For each MT catastrophe at the cortex, the average pulling forces acting on a single MT at the posterior are stronger than those at the anterior, due to the different probabilities of MT-force generator interactions (see Materials and methods). Error bars show 95% CI. Double asterisk and n.s. indicates:  $p < 0.01$  and  $p > 0.05$  compared to control (Kruskal-Wallis test followed by Dunn's multiple comparison test). Scale bars indicate  $5 \mu\text{m}$ .

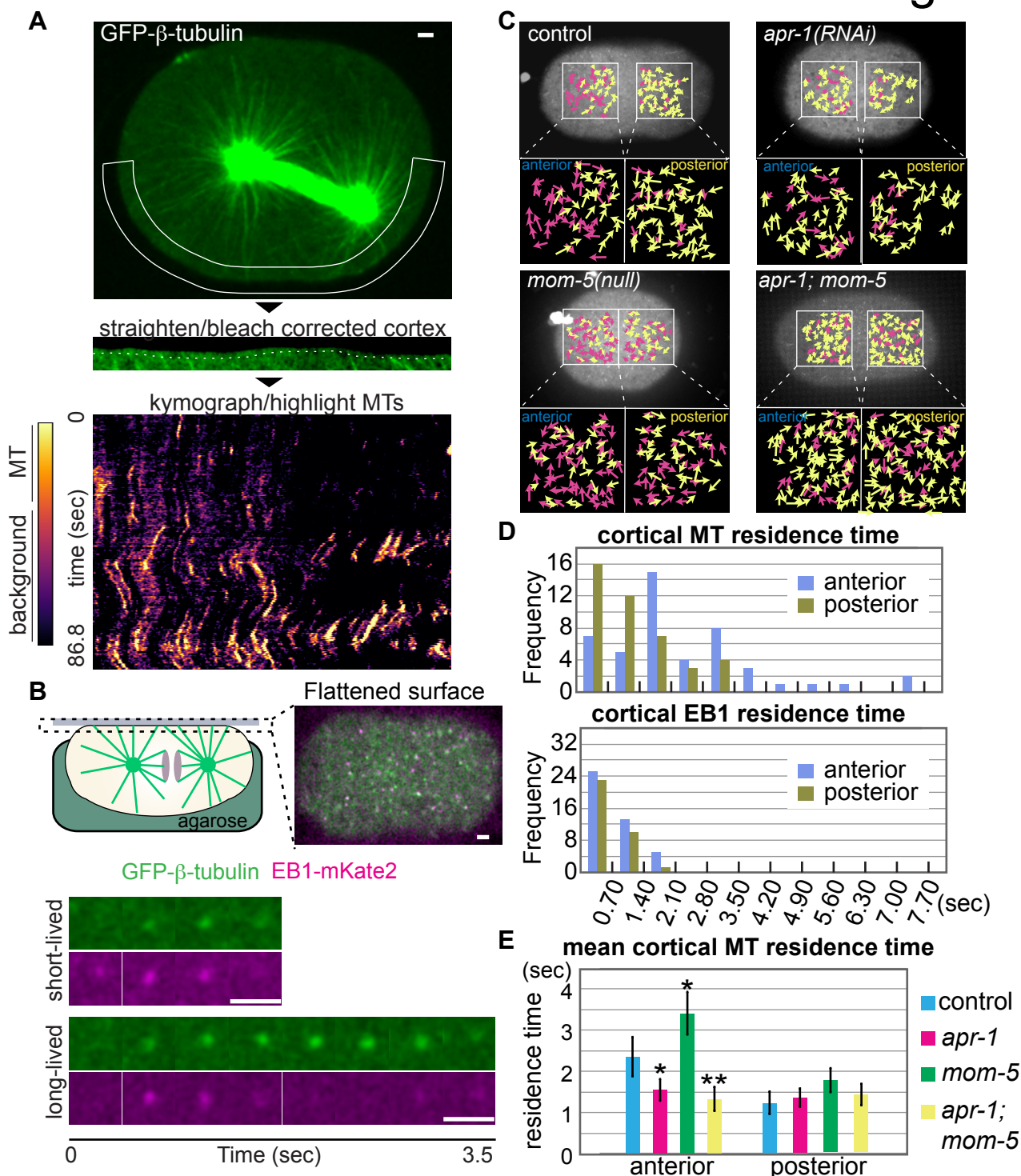


**Figure 3. APR-1 asymmetrically stabilizes microtubule-cortex interactions.**

(A) Cortical MT dynamics. Cortical area outlined by the solid line in top figure was extracted, straightened, and corrected for photobleaching. This cortical area, depicted by the dotted line (middle), was used to generate a kymograph (bottom). Color code of the kymograph was changed to highlight MTs. (B) Measurement of cortical MT residence. The embryos were mounted on agarose pads and flattened by coverslips to visualize cortical microtubule ends in a single focal plane. Examples of short and long-lived foci were shown below with simultaneous imaging of GFP:: $\beta$ -tubulin and EB1::mKate2. (C) Cortical microtubule dots in the indicated genotypes during metaphase-anaphase. Images are max projection of cortical GFP:: $\beta$ -tubulin for 60 frames (42 sec). Yellow and Magenta arrows indicate the MT dots whose residence time was shorter and longer than 2.1 sec, respectively. See also Video 3, 5-7. (D) Distribution of quantified cortical MT or EB1 residence time in wild-type animals. (E) Mean cortical MT residence time of indicated genotypes.  $n = 47, 42, 77, 67, 64, 61, 37, 44$ , from left to right. Error bars show 95% CI. Double asterisk and asterisk indicate:  $p < 0.01$  and  $p < 0.05$  compared to control (Kruskal-Wallis test followed by Dunn's multiple comparison test). Scale bars indicate  $2.5 \mu\text{m}$ .

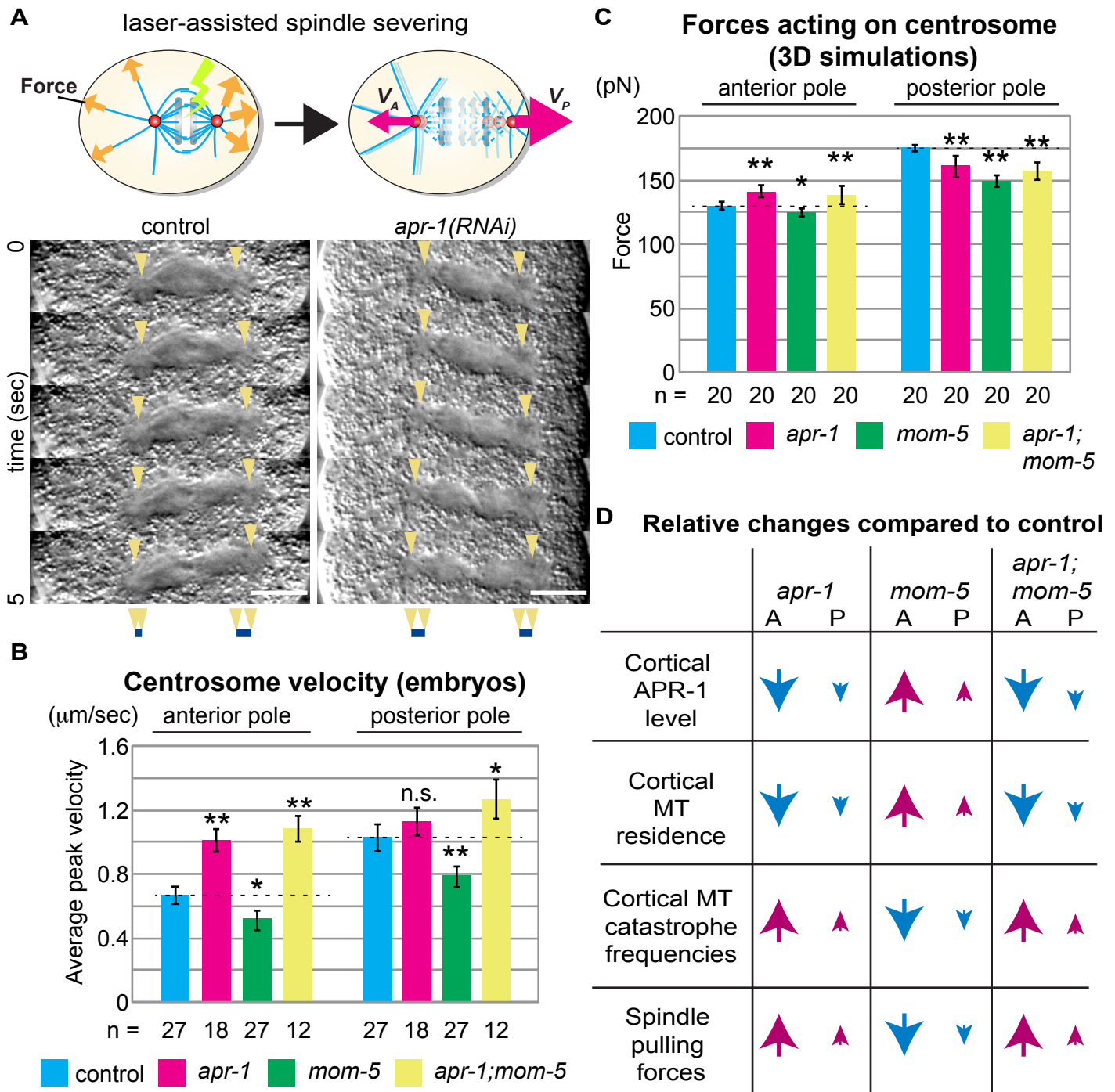


**Figure 4 APR-1 asymmetrically attenuates pulling forces acting on the mitotic spindle.**

(A) Spindle severing experiments. The midzones of mitotic spindles were severed by laser irradiation around anaphase onset (upper left panel). Upon spindle severing, spindle remnants moved at different velocities depending on the net strength of pulling forces (upper right panel). Montages of dissected spindle dynamics were shown in the bottom panels as DIC images; spindle poles devoid of yolk granules were indicated by arrowheads. (B) Average peak velocity of spindle poles after spindle severing. (C) The average of outward pulling forces over 5 sec from anaphase onset ( $t = 100$  s) for 20 independent simulations. Error bars show 95% CI. Double asterisk and asterisk indicate:  $p < 0.01$  and  $p < 0.05$  compared to control (one-way ANOVA with Holm-Sidak's method). (D) Summary of relationships between cortical APR-1 level, cortical MT residence, cortical MT catastrophe frequencies, and spindle pulling forces. Scale bars indicate 10  $\mu$ m.



## Figure 5

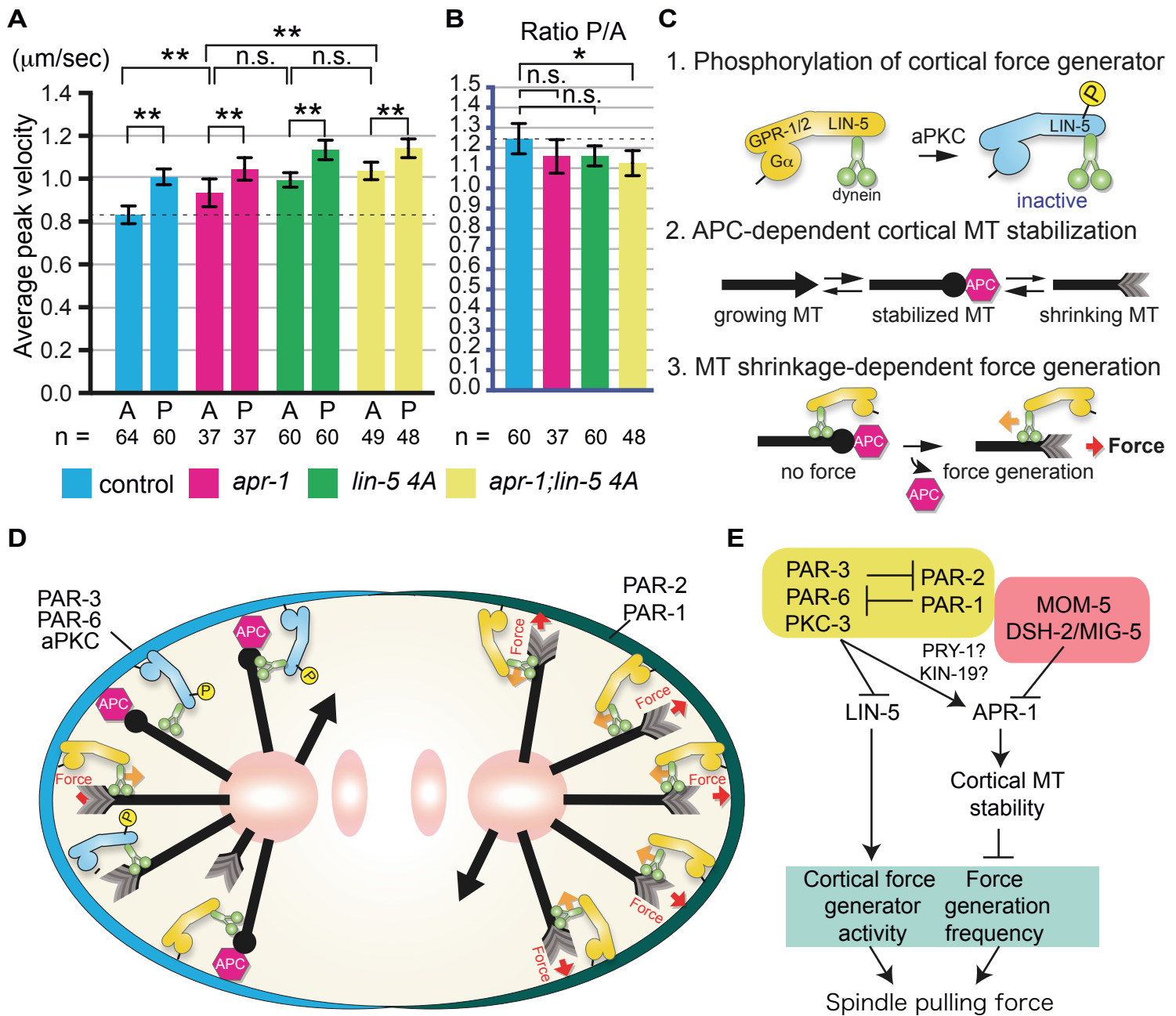


**Figure 5 Anterior APR-1 enrichment and LIN-5 phosphorylation together attenuate spindle pulling forces to generate pulling force asymmetry.**

(A, B) Average peak velocity of spindle poles (A) and their posterior/anterior ratio (B) after spindle severing. Error bars show 95% CI. Double asterisk and asterisk indicate:  $p < 0.01$  and  $p < 0.05$  compared to control (one-way ANOVA with Holm-Sidak's method). (C) Three elementary processes used in the model described in the panel C. (1) aPKC-dependent LIN-5 phosphorylation results in the inhibition of force generation, (2) Cortical MT stabilization by APC reduces the MT catastrophe frequency and (3) MT shrinkage-dependent force generation is suppressed by step (2). (D) A schematic model of asymmetric spindle force regulation in P0 cell (see text). (E) A diagram of spindle pulling force regulation pathways at the anterior cell cortex.